Neurotoxicity Research (2025) 43:13
https://doi.org/10.1007/s12640-025-00737-3

RESEARCH

# Multi-Omics Analysis of Hippocampus in Rats Administered Trimethyltin Chloride

**Douaa Zakaria**[1,2] · **Tomoki Yamashita**[1] · **Yohei Kosugi**[1]

Received: 7 January 2025 / Revised: 5 March 2025 / Accepted: 10 March 2025 / Published online: 17 March 2025


## Abstract

Trimethyltin chloride (TMT) is a neurotoxicant that damages the central nervous system (CNS) and triggers neurodegeneration. This study used multi-omic data, including transcriptomics and proteomics of the rat hippocampus, to identify differentially expressed genes and proteins in TMT-induced neurotoxicity over time, related to neuro-axonal damage marked by plasma Neurofilament Light (NfL) levels. Data were collected at 12, 24, 48, 72, and 168 h post-TMT administration. NfL levels surged at 72 and 168 h, confirming neuro-axonal damage. Transcripts of genes in the chemokine signaling pathway (Cxcl10, Cxcl12, Cxcl14, Cxcl16), apoptosis pathway (Caspase-3, PARP1, CTSD), and TNF signaling pathway (TNFR1, MMP9, ICAM-1, TRAF3) showed significant differential expression starting from 48 h, preceding the NfL increase, suggesting their roles in neuro-axonal damage. Additionally, 11 Alzheimer's disease-related proteins, with significant changes from 72 to 168 h, were detected only in the proteomic dataset, indicating post-translational modifications might be crucial in neurotoxicity. Pathway analysis revealed that neurodegeneration and Alzheimer's disease pathways were among the top 15 affected by TMT-induced gene regulation, aligning with the involvement of TNF signaling, apoptosis, and chemokine signaling in neurodegeneration. This research highlighted the value of longitudinal omics studies, combined with pathway enrichment, gene-disease association, and neuro-axonal damage biomarker analyses, to elucidate neurotoxicant-induced neurodegeneration. Findings from this study could enhance the understanding of TMT-induced neurotoxicity, potentially informing future therapeutic strategies and preventive measures.

**Keywords** Transcriptomics · Proteomics · Trimethyltin · Neurotoxicant · Neurotoxicity

## Introduction

Trimethyltin chloride (TMT) is a highly effective neurotoxic agent frequently employed in the study of neurotoxicity (Imam et al. 2017; Ogata et al. 2014), neuroinflammation (Hou et al. 2018), and neurodegeneration (Geloso et al. 2011). It specifically targets the limbic system, with a pronounced effect on the hippocampus, resulting in neuronal death and behavioral deficits including hyperactivity, cognitive impairment, and spontaneous seizures. Additionally, it induces biochemical alterations that are similar to those observed in neurodegenerative diseases, such as Alzheimer's (Geloso et al. 2011; Lee et al. 2016). Comprehending the mechanisms underlying TMT-induced neurotoxicity is crucial, given its significance in the modeling of neurodegenerative diseases, its potential risks to environmental and occupational health, and its ramifications for the advancement of therapeutic strategies (Geloso et al. 2011; Lee et al. 2016; Kurkowska-Jastrzebska et al. 2007).

TMT-induced neurotoxicity exhibits distinct patterns across species and exposure models, reflecting differences in hippocampal vulnerability (Lattanzi et al. 2013). In mice, TMT toxicity predominantly affects granule cells in the dentate gyrus, leading to rapid neuronal damage at lower doses (Chang et al. 1983). In rats, TMT primarily targets pyramidal neurons in the CA3 region, with progressive neuronal

✉ Yohei Kosugi
youhei.kosugi@takeda.com

Douaa Zakaria
douaazakaria0@gmail.com

Tomoki Yamashita
tomoki.yamashita1@takeda.com

[1] DMPK&Modeling, Takeda Pharmaceutical Company Limited, 26-1 Muraoka-Higashi, 2-Chome, Fujisawa, Kanagawa 251-8555, Japan

[2] The Graduate University for Advanced Studies, SOKENDAI, Miura, Kanagawa, Japan

death overtime (Geloso et al. 2011). The choice of TMT administration protocol further influences the extent and severity of neurotoxicity. Chronic exposure models, which involve repeated dosing over multiple days or weeks, result in longer-lasting neurodegeneration, whereas acute exposure models, which use a single-dose administration, allow for the study of early molecular and cellular responses (Lattanzi et al. 2013). This study employs an acute TMT administration model, where a single oral dose (10 mg/kg) was administered to rats, followed by analysis at multiple time points (12–168 h post-exposure). This approach enables the investigation of the initial molecular events leading to neuro-axonal damage, including gene and protein expression changes linked to synaptic dysfunction, neuroinflammation, and neuronal degeneration.

In a number of neurological conditions, including multiple sclerosis, amyotrophic lateral sclerosis, Huntington's disease, and Alzheimer's disease, neurofilament light (NfL) is a novel biomarker and clinical marker that indicates the severity, course, or responsiveness to therapy (Gaetani et al. 2019; Kuhle et al. 2016) Recent advancements in single-molecule array technology (Simoa) have made it possible to monitor blood NfL levels with high accuracy and sensitivity (Kuhle et al. 2016; Khalil et al. 2018). Sano et al. (2021) demonstrated that TMT exposure in rats causes significant NfL elevations in serum and cerebrospinal fluid (CSF), which correlate with hippocampal neuronal degeneration and glial activation (Sano et al. 2021). Histopathological findings revealed progressive CA3 neuronal loss, accompanied by astrocytosis (marked by increased GFAP expression) and microglial activation (evidenced by Iba1 staining). Astrocytic reactivity appeared within 48 h post-TMT, while microglial activation peaked between 72 and 168 h, suggesting a role in secondary neurotoxicity through inflammatory responses (Sano et al. 2021).

Several studies have indicated that TMT induces neurodegeneration through the activation of specific genes within the tumor necrosis factor (TNF) signaling pathway (Little et al. 2002), reactive oxygen species pathways (Corvino et al. 2005; Edalatmanesh et al. 2015; Kaur et al. 2013; Shin et al. 2005), apoptosis (Kurkowska-Jastrzebska et al. 2007; Ceccariglia et al. 2011), and the chemokine signaling pathway (Little et al. 2002). For instance, a study investigating TMT administration and Cathepsin D (Cat D), a lysosomal protease associated with apoptosis and neuronal loss, employed enzymatic activity assays and immunohistochemical localization to find that TMT administration resulted in neuronal loss and elevated levels of Cat D activity in astrocytes, microglial cells, and CA3 neurons within the rat hippocampus (Ceccariglia et al. 2011). A separate investigation employed immunocytochemistry to demonstrate that TMT administration led to initial oxidative stress, seizures, and a sustained disturbance of glutathione homeostasis in the rat brain (Shin et al. 2005). The isolation of RNA and PCR targeting monocyte chemoattractant protein (MCP)−1 in a separate study indicated that TMT resulted in significant elevations of hippocampal-derived MCP-1, which may play a signaling role in the compromised central nervous system (Little et al. 2002).

Nevertheless, current research on TMT-induced neurodegeneration has predominantly relied on biochemical assays and targeted RNA assays to investigate a particular set of genes (Kurkowska-Jastrzebska et al. 2007; Little et al. 2002; Corvino et al. 2005; Edalatmanesh et al. 2015; Kaur et al. 2013; Shin et al. 2005; Ceccariglia et al. 2011), or has utilized proteomic data to analyze the general responses across various phases of cell maturation (Schvartz et al. 2019), without delving into the specific functions of certain pathways and their differentially expressed genes in the context of neural damage (Schvartz et al. 2019). To put it differently, none of the research undertaken to date has examined time-based TMT-induced neurotoxicity through the lens of multi-omic data concerning the timing of neural damage, with the objective of offering a thorough overview of TMT-induced neuro-axonal damage and the genes responsible for it.

This research employed multi-omic data, encompassing transcriptomic and proteomic analyses of the hippocampus in TMT-treated rats, to identify temporal patterns of TMT-induced gene/protein expression associated with neuro-axonal damage, as indicated by NfL levels. By integrating these data, we identified several differentially expressed genes and proteins associated with neurotoxicity, both prior to and following neuro-axonal damage, emphasizing the pathways and genes implicated in TMT-induced neuro-axonal damage. This study underscored the significance of integrating multi-omic data with the evaluation of neuro-axonal damage biomarkers and pathway enrichment analysis to elucidate the mechanisms by which environmental toxicants, such as TMT, may induce neuro-axonal damage, particularly in the context of neurodegenerative diseases like Alzheimer's. This approach could inform future therapeutic strategies and preventive interventions.

## Materials and Methods

### Materials

TMT Chloride was purchased from Tokyo Chemical Industry Co., Ltd. (Tokyo, Japan). All other reagents and solvents were of analytical grade or better and were commercially available.

## Animal Study

The study involved animals and administrations that were approved by the Institutional Animal Care and Use Committee at BoZo Research Center, Inc. (Shizuoka, Japan). The test facility, Gotemba laboratory of BoZo Research Center, Inc. is fully accredited by the AAALAC International. Forty male F344/DuCrlCrlj rats (Jackson Laboratories Japan Inc.) weighing between 193 and 223 g were used (8 weeks). These animals were divided into 10 groups, each consisting of 4 males. The rats were housed in metal cages with stainless-steel wire mesh bottoms, equipped with a stainless-steel resting board and chew toys for animal enrichment. The room conditions included a temperature range of 20–26 °C, a relative humidity range of 30–70%, air exchange of 10–15 times per hour, and a 12-h light/dark cycle. The animals had ad libitum access to a pelleted laboratory animal diet (CRF-1, ORIENTAL YEAST CO. LTD., Tokyo, Japan) and tap water. TMT Chloride was diluted with distilled water and was orally administered at a dose of 10 mg/5 mL/kg to five groups so that the total number of TMT-treated rats is 20 rats. The five other groups were given distilled water alone in the same manner, so that the total number of control rats is 20. At various time points (12, 24, 48, 72 and 168 h after administration), one TMT-treated group and one control group were sacrificed. The samples at each time point consisted of four replicates, except for the 72-h group, which included only three rats due to an animal fatality. Although the number of replicates is small, this is mitigated by the consideration that the rats were housed under the same conditions and that the study is a time-course experiment. The abdomen was opened under isoflurane inhalation anesthesia. Blood samples (1 mL) were collected from the abdominal aorta using a syringe with anticoagulant (3% [v/v] 0.1 M EDTA-2Na) and then centrifuged at 18,000 × g for 1 min to obtain plasma for NfL assay. After draining the blood sufficiently, a whole-body cardiovascular perfusion was conducted using heparinized PBS (Phosphate Buffered Saline) injected through the heart. The brain was excised, and the right hippocampus was dissected. The right hippocampus was further divided into halves, with each half used for transcriptomic and proteomic assays, respectively. All samples were stored at −80℃ until analysis. The dosage levels for TMT were determined based on doses reported in the literature (Sano et al. 2021). Clinical signs were monitored daily, and body weight was measured on days 1, 2, 3, and 7. In the TMT-treated group, irritability was observed in a small number of animals 48 h post-administration and in all animals 72 h post-administration. Muscle spasms were observed in a small number of animals 72 h post-administration and in many animals from 96 h post-administration. Additionally, a decrease in spontaneous movement activity was observed in a small number of animals in the TMT-treated group 168 h post-administration.

## Quantitation of NfL

NfL levels in rat plasma were assessed by employing a Simoa HD-X analyzer (Quanterix Corporation, Massachusetts) along with a Simoa NF-light Advantage (HD-X) Kit (Quanterix, cat. no. 104073), following the instructions provided by the manufacturer. Plasma samples were diluted at a 1:3 ratio for all assays. A seven-point calibration curve and sample concentrations were determined on the Simoa HD-X analyzer software using a weighting factor of $1/y^2$. All samples were tested in duplicate and analyzed using the same batch of kits.

## Transcriptomic Analysis

The experiment was conducted by Takara Bio Inc. Half of hippocampus was homogenized by TissueLyser II (Qiagen Inc.) with Lysis Buffer RA1 based on the instruction of NucleoSpin RNA (Takara Bio Inc., cat. no.740955). The SMART (Switching Mechanism At 5' End of RNA Template) method was used to attach adapter sequences to both ends of the 1st strand cDNA according to the manufacturer's instructions of a SMART-Seq v4 Ultra Low Input RNA Kit (Clontech). The PCR amplification was performed using a primer that recognizes the attached adapter sequences, and the resulting PCR products were purified using AMPureXP (Beckman Coulter). These purified products were then used as double-stranded cDNA amplification products. Subsequently, tagmentation reaction using transposons was performed to fragment the double-stranded complementary DNA (cDNA) and add adapter sequences to both ends. PCR amplification was carried out using primers with indexes that recognize the adapter sequences and have different tag sequences for each sample, resulting in the creation of sequence libraries with added indexes. The quality of the constructed sequence libraries was assessed using an electrophoresis apparatus. The constructed library was sequenced using NovaSeq 6000 (Illumina) and the sequencing data was mapped to the reference genome sequence for transcript-level expression analysis.

## Proteomic Analysis

10% homogenate of hippocampus was prepared by 4% SDS with protease inhibitors (Complete, Roche, cat. no. 04 693 132 001; PhosStop, Roche, cat. no. 04 906 837 001) and sonicated for 5 min. After incubation at 95℃ for 10 min, protein concentrations were determined using BCA assay kit (Thermo Fisher Scientific, cat. no. 23225). 100 µg protein

(20 µL) was mixed with 1 M phosphoric acid buffer (5 to 1 mixture of 1 M $NaH_2PO_4$ and 1 M $Na_2HPO_4$, 10 µL), 5 M NaCl (5 µL) and cold acetone (0.5 mL) at −30℃ for overnight. After centrifugation (15,000 rpm, 4℃, 20 min), the supernatant was completely removed, and the precipitant was kept at room temperature for 15 min. The precipitant was solved by 8 M Urea (FUJIFILM Wako, cat. no. 219–00175), 0.5 M TCEP (Thermo Fisher Scientific, cat. no. 77720), and 0.5 M Iodoacetamide (Thermo Fisher Scientific, cat. no. A39271) with sonication (10 min) and then incubated for 10 min at 37℃. Proteolytic digestion was conducted using 1 µg of LysC (FUJIFILM Wako, cat. no. 283–95481) for 2 h at 37℃ and then using 1 µg of Trypsin (Promega, cat. no. XV528) for overnight at 37℃. After adding 4% phosphoric acid, the sample was centrifuged at 3,000 rpm for 15 min. Supernatant was applied to Oasis MCX (Waters) and the final eluted solution was dried up. After reconstituted with 4% acetonitrile/0.1% formic acid solution (50 µL) was added with vortex 10 min. After sonication for 5 min, an aliquot of 20 µL was transferred to vial and an aliquot of 1µL was injected into EASY-nLC 1200/QExactive HF-X (Thermo Fisher Scientific) and analyzed in data-independent acquisition (DIA) mode. LC buffers were prepared as follows: buffer A (0.1% formic acid in water (v/v)) and buffer B (80% acetonitrile and 0.1% formic acid in water (v/v)). An NTCC-360/75–3–15 analytical capillary column (3 µm, 0.075 mm i.d. × 150 mm, Nikkyo Technos) along with an Acclaim PepMap 100 C18 trap column (3 µm, 0.075 mm i.d. × 20 mm, Thermo Fisher Scientific) was used at room temperature. The peptides were eluted from the column at a constant flow rate of 300 nL/min using a linear gradient. The gradient started at 5% buffer B and increased to 30% buffer B over 30 min. It then progressed from 30% buffer B to 50% buffer B over 8 min, followed by a transition from 50% buffer B to 100% buffer B over 7 min, and finally washing with 100% buffer B within 10 min. The mass spectra were obtained in positive ion mode under the following conditions: a resolving power of 30,000 and 15,000 (full width at half maximum) for MS1 full scan and DIA, respectively, an automatic gain control (AGC) target of 3,000,000 and 1,000,000 for MS1 full scan and DIA, respectively, a spray voltage of 2.00 kV, a capillary temperature of 275 °C, and a funnel RF level of 45.0.

## Statistical Analysis and Data Processing

For the transcriptomic dataset, first a t-test was performed on each measurement to compare the log2 ratios of the 4 treated replicates and 4 control replicates. Following this, the difference between the average log2 ratios of the 4 treated replicates and the average log2 ratios of the 4 control replicates was calculated for each measurement. Then, for multiple test correction, the Benjamini & Hochberg method (BH method) was used. Finally, genes that have a *Q*-value of t-test (false discovery rate threshold) less than 0.05 and an absolute average log2 ratio (representing fold change) greater than 0.58 were classified as differentially expressed genes.

For the proteomic dataset, a spectral library was generated in DIA-NN using FASTA file (UniProt Reference Proteome, Taxonomy 10,116, unreviewed sequences, 54,767 entries, downloaded on 2023.02.17). The trypsin enzyme parameter was set to allow one potential missed cleavage. Carbamidomethylation of cysteines was set as a fixed modification, and the toggle for N-terminal methionine removal was turned on. Peptide and protein identifications were filtered at a 1% False Discovery Rate (FDR). Spectronaut v17.6 (Biognosys AG) was used with the spectral library generated by DIAN-NN for DIA analysis using the default search parameters. Carbamidomethylation of cysteines was set as a fixed modification. Peptide and protein identifications were filtered at 1% FDR. Similar to the transcriptomic analysis, proteins showing a *Q*-value of less than 0.05 and an absolute average log2 ratio greater than 0.58 were classified as differentially expressed proteins.

In order to match transcriptomic and proteomic datasets, the UniProt IDs of the proteomic dataset were converted to their corresponding gene Kyoto Encyclopedia of Genes and Genomes (KEGG) IDs using bioservices and the Uniprot API (Cokelaer et al. 2013). Meanwhile, the Ensembl transcript IDs of the transcriptomic dataset were converted first to Entrez gene IDs, then to gene KEGG IDs using Mygene API (Lelong et al. 2022; Wu et al. 2012; Xin et al. 2016). Then KEGG IDs from both datasets were merged and used for the correlation analysis and KEGG multi-omics visualization.

## KEGG-Related Visualization

A dataset containing all KEGG pathways of *Rattus norvegicus*, along with the genes present in each pathway, was prepared using bioservices and the KEGG API (Cokelaer et al. 2013). The differentially expressed genes/proteins from both transcriptomic and proteomic datasets were searched against the Rattus norvegicus KEGG pathway dataset to determine the number and percentage of differentially expressed genes/proteins in each pathway at each time point. Subsequently, the number and percentage of differentially expressed genes/proteins across all time points were calculated for each pathway. Finally, the dataset was sorted based on the percentage of differentially expressed genes/proteins across all time points to identify the top 20 KEGG pathways.

The KEGG API (Cokelaer et al. 2013) was utilized to display the average log2 ratio values on KEGG pathway diagrams, with upregulated genes/proteins shown in blue and downregulated genes/proteins shown in red. It is important

to mention that the intensity of the color varies based on the average log2 ratio value.

Finally, transomics2cytoscape (Nishida et al. 2024) was used to visualize the consistency of results between transcriptomic and proteomic data.

### Gene-Disease Association (GDA) Score

The gene-disease association (GDA) was investigated by Open Targets Platform (Ochoa et al. 2022) and DISGENET plus (Piñero et al. 2019). Open Targets Platform generates various types of scores to represent GDAs based on evidence, including genetic associations, somatic mutations, drugs, pathways and systems biology, text mining, RNA expression, and animal models (Ochoa et al. 2022). DISGENET plus also generates Gene-Disease Association (GDA) score based on associations reported by several databases, including Genome Wide Association Studies (GWAS), ClinGen, Genomics England panel app, etc. (Piñero et al. 2019). Default parameters were used in the database search.

### Similarity Search of Transcriptomic Data Using Analysis Match

Analysis Match, which is a function of QIAGEN Ingenuity Pathway Analysis (IPA), automatically searches for other transcriptomics expression profiles that have similar or opposite biological outcomes to one's own transcriptomics expression profile. This search is based on expression analysis results derived from public databases and performs comparative analysis based on matching results with canonical pathways, upstream regulators, causal networks, diseases, and function analysis results, as well as common patterns in datasets. The analysis used for Analysis Match included expression analysis results related to human and mouse diseases/cancers available in the Sequence Read Archive (SRA), Gene Expression Omnibus (GEO), Array Express, The Cancer Genome Atlas (TCGA), Library of Integrated Network-Based Cellular Signatures (LINCS), and other databases. Default parameters were used in the database search.

### Weighted Gene Co-Expression Network Analysis (WGCNA)

Weighted Gene Co-expression Network Analysis (WGCNA) was performed using the WGCNA R package (Langfelder and Horvath 2008) on 6013 transcripts that corresponded to DEGs ($Q$-value $< 0.05$, absolute average Log2 of fold change $> 0.58$). Using the goodSamplesGenes function with the default settings, no outlier genes were found. To ensure that there were no outlier samples, hierarchical clustering was employed. The optimum soft-threshold power was then found by using the pickSoftThreshold function, fitting a scale-free topology model, and creating mean connectivity charts. Since 9 is the lowest power at which the scale-free topology fit is greater than 0.8, it was selected as the soft threshold power. Next, a dissimilarity matrix of the Topological Overlap Matrix (TOM) was produced. Linkage hierarchical clustering was then used to group the dissimilarity measures. After identifying the Module Eigengene (ME), the clusters (branches) were further reduced to more meaningful modules by clustering the modules according to pairwise eigengene correlations. Modules with expression profiles that were more than 70% identical were then merged. A gene dendrogram was created that displays the colors of the original and combined modules. After that, a heatmap illustrating the module-trait link was made utilizing the Pearson correlation for time, dose, and NfL characteristics. Lastly, because black and green-yellow modules showed a positive connection with time, dosage, and NfL, the module membership (MM) of their genes as well as their gene significance (GS) with NfL was computed. Genes that had MM > 0.8 and GS > 0.5 were classified as driving genes.

## Results

### Plasma NfL Levels Over Time

The time profile of plasma NfL levels in rats with and without TMT was investigated in Fig. 1. Plasma NfL levels were increased over time and showed a 31- and 145-fold increase at 72 and 168 h after oral administration of TMT, respectively.

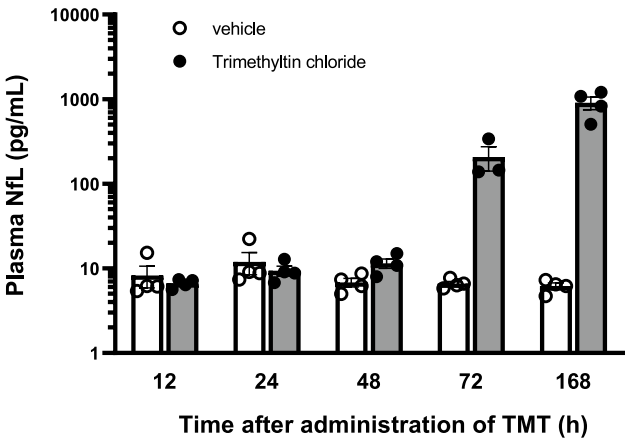


**Fig. 1** Time profile of plasma NfL concentrations in rats after oral administration of TMT. White bars represent the vehicle group, and solid gray bars represent the TMT-administrated group

## Differentially Expressed Genes/Proteins Over Time

In transcriptomic analysis, the number of differentially expressed genes increased over time, with a relatively even distribution of upregulated and downregulated genes at each time point (Fig. 2a). When examining the transitions between time points, it was clear that most genes either maintained their regulation status or became nonsignificant (Fig. 2). Observing the regulation patterns over time, we found that 188 genes remained upregulated and 174 genes remained downregulated from 48 to 168 h post TMT administration (Fig. 3a). Additionally, the highest number of upregulated and downregulated genes was observed at 72 and 168 h post TMT administration (Fig. 2a). Notably, there were over 669 genes uniquely down regulated at 72 h after TMT administration and 675 genes uniquely up regulated at 168 h after TMT administration (Fig. 3a).

At the proteomic level, we observed comparable proportions of upregulated and downregulated proteins at each time point, with the highest number of upregulated and downregulated proteins seen at 72 and 168 h post TMT administration (Fig. 2b). Additionally, there was a significant number of uniquely down regulated proteins at 72 h (147 proteins) and uniquely upregulated proteins at 168 h (146 proteins), like the transcriptomic data (Fig. 3b). However, in contrast to transcriptomic data, there was a noticeable presence of upregulated and downregulated proteins even at 12 and 48 h post TMT administration (Fig. 2).

Upon examining the correlation between transcriptomic and proteomic data, it became evident that the proteomic findings at 168 h after TMT administration exhibit a strong positive correlation with the transcriptomic data at 48, 72, and 168 h post TMT administration (Fig. 4a). This could be attributed to the cellular stress response, wherein the cell focused on the production of proteins that are crucial for

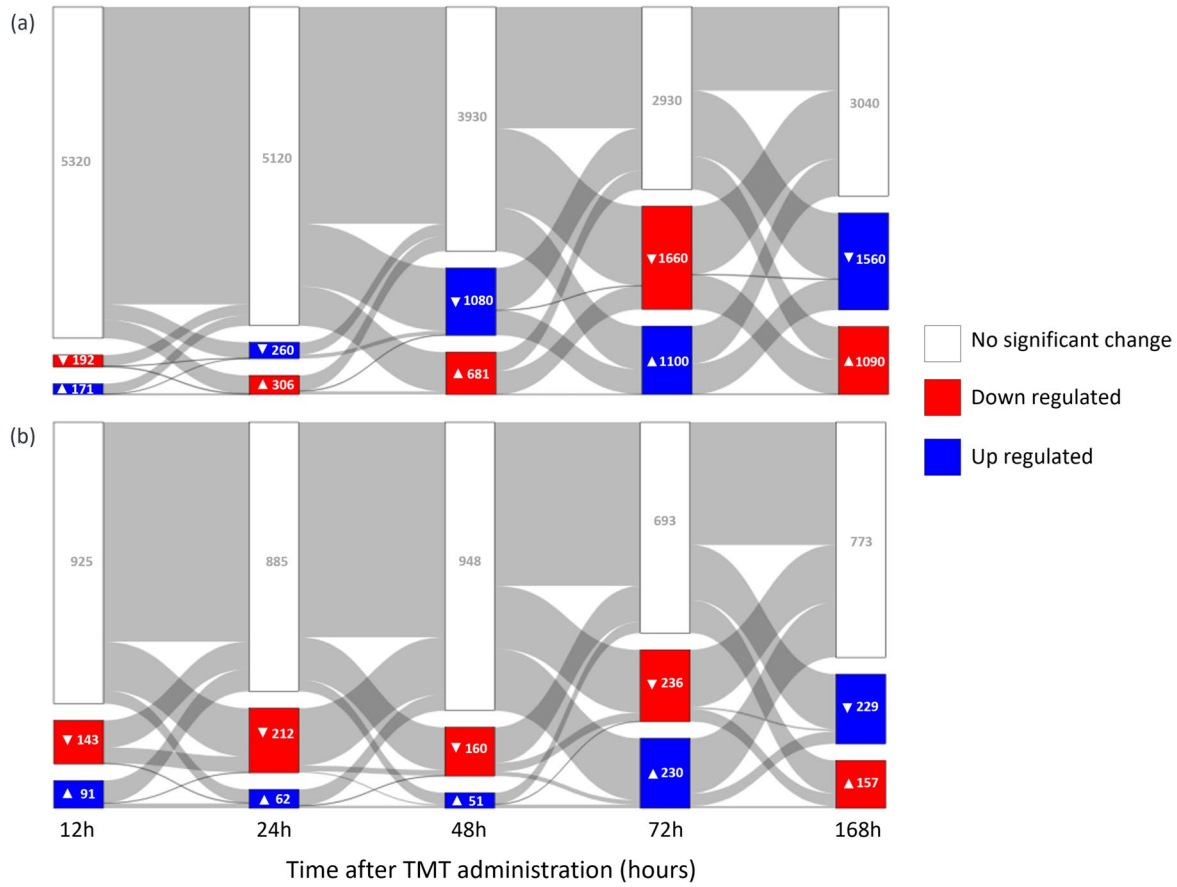


**Fig. 2** Sankey diagram illustrating the temporal dynamics of differentially expressed genes (DEGs) in transcriptomic (**A**) and differentially expressed proteins (DEPs) in proteomic (**B**) datasets at all time points following TMT administration. Unlike bar graphs that only show the number of DEGs per time point, the Sankey diagram allows for the visualization of gene and protein expression changes over time by mapping transitions between states. Each bar is labeled with the number of genes or proteins at that time point. Upregulated genes/proteins are represented by blue bars and an upward-pointing triangle (▲), downregulated genes/proteins are represented by red bars and a downward-pointing triangle (▼), and those with no significant change are shown in white. The width of each flow corresponds to the number of genes or proteins transitioning between states across time points

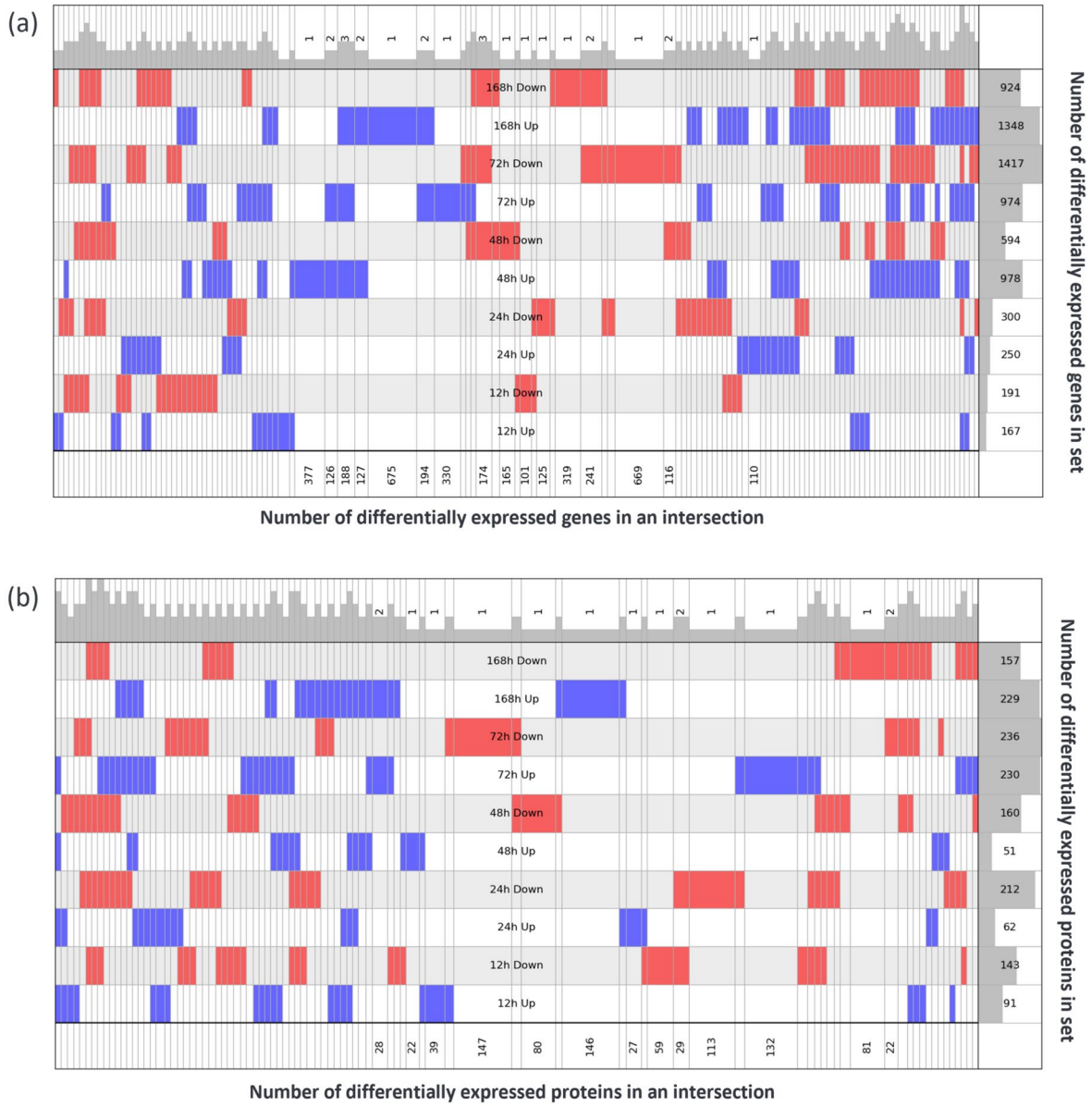


**Fig. 3** Supervenn diagram of differentially expressed genes/proteins in transcriptomic (**a**) and proteomic (**b**) data over time. Sets are represented horizontally, and intersections are represented vertically. Each number on bottom represents the number of DEGs/DEPs in an intersection, and the annotation for these numbers is limited to intersections that have 100 DEGs in (a) and 20 DEPs in (b) for clearer representation. Each number on the right represents the number of genes/proteins in a set. Sets are ordered chronologically according to the time point after TMT administration. Blue intersections represent up regulated genes/proteins, and red intersections represent down regulated genes/proteins. Blue and red blocks in a row indicate that this row is part of the intersection, while gray and white blocks indicate that the row is out of intersection

managing damage, rather than regulating or suppressing other proteins (Vogel and Marcotte 2012).

Looking at the intersections between transcriptomic and proteomic data, we can see 31 DEGs/DEPs corresponding to the same genes at 168 h after TMT administration. In addition, there are 26 genes that were DEGs from 48 to 168 h after TMT administration and DEPs at 168 h after TMT administration (Fig. 4b).

## Differentially Expressed Genes/Proteins in KEGG Pathways

Upon analysis of the differentially expressed genes/proteins at various time points, it was noted that neurodegeneration and Alzheimer's disease pathways were among the top 15 KEGG pathways in both the transcriptomic and proteomic datasets (Online Resource 1, 2). At the transcriptomic level,

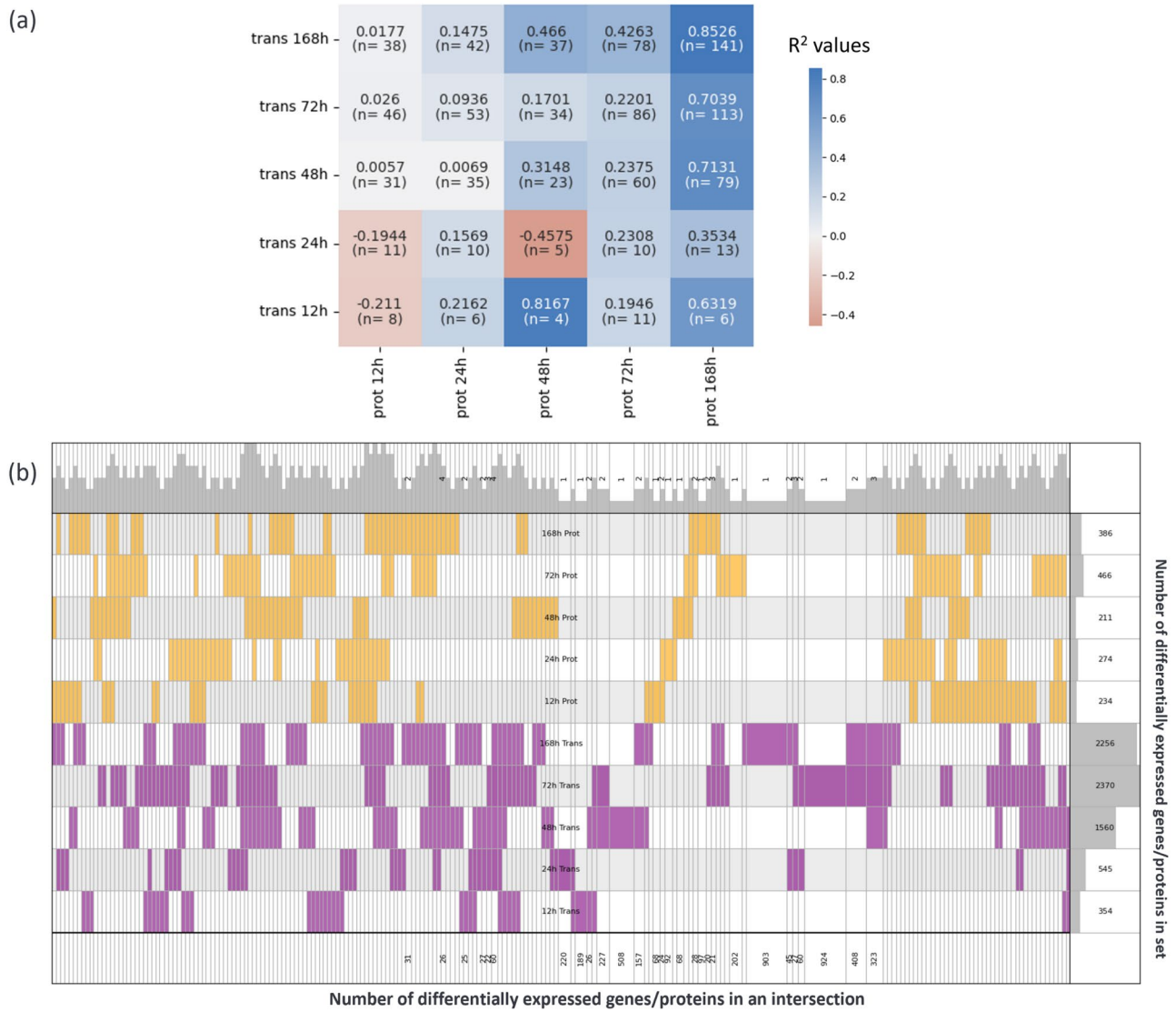


**Fig. 4** The interplay between transcriptomic and proteomic data at all time points after TMT administration. (**a**) Heatmap of correlation analysis between transcriptomic and proteomic data at all time points after TMT administration. $R^2$ values are calculated with the number of data points written in parenthesis. (**b**) Supervenn diagram of differentially expressed genes/proteins in transcriptomic and proteomic data over time. Sets are represented horizontally, and intersections are represented vertically. Each number on bottom represents the number of DEGs/DEPs in an intersection, and the annotation for these numbers is limited to intersections that have 20 DEGs/DEPs for clearer representation. Each number on the right represents the number of genes/proteins in a set. Sets are ordered chronologically according to the time point after TMT administration. Purple intersections represent DEGs, and orange-yellow intersections represent DEPs. Gray and white blocks in a row indicate that the row is out of intersection

starting from 48 h post-TMT administration, a substantial number of genes, ranging from 20 to over 40, exhibited significant differential expression in pathways like TNF signaling, reactive oxygen species, apoptosis, and chemokine signaling pathways (Fig. 5a). Moreover, around 30 to 50 genes showed differential expression in pathways linked to Alzheimer's disease, Huntington's disease, Prion disease, and Parkinson's disease (Fig. 5). Conversely, in the proteomic dataset, the number of differentially expressed proteins was notably lower. However, there was a marked increase in the number of differentially expressed proteins at 72 h post-TMT administration (Fig. 5b).

As the neurodegeneration pathway was among the top 15 pathways affected by TMT-neurotoxicity, the concurrence of transcriptomic and proteomic data in neurodegeneration pathways was observed at the 72-h mark. It became evident that there were only a handful of conflicting results in terms of regulation type (Fig. 6). However, there were a few genes/proteins that exhibited differential expression at both the transcriptomic and proteomic levels simultaneously. This

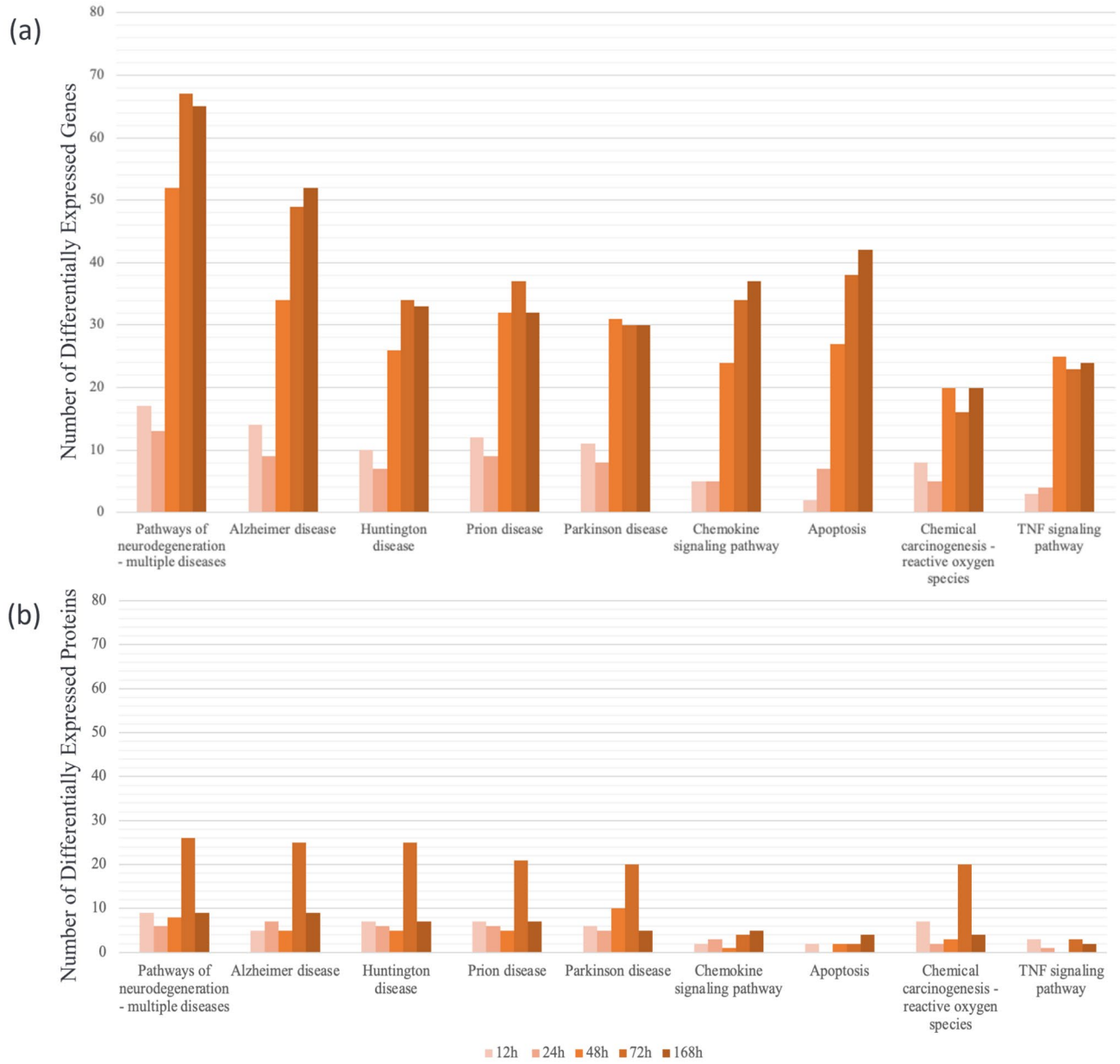


**Fig. 5** Bar plots of differentially expressed genes/proteins in neurodegeneration related KEGG pathways from transcriptomic (**a**) and proteomic (**b**) data at all time points after TMT administration. The bar's color intensity is based on the time point after TMT administration

observation was evident when analyzing the dark blue and dark red lines, which represented upregulated and downregulated genes/proteins in both transcriptomic and proteomic datasets, respectively (Fig. 6). Additionally, looking at the proportion of red to blue lines in Fig. 6, we could see that the proportions of upregulated and downregulated genes/proteins were relatively similar.

To date, several pathways such as TNF signaling, reactive oxygen species pathways, apoptosis, and chemokine signaling pathways have been documented in TMT-induced neurodegeneration (Lee et al. 2016). By examining these diverse KEGG pathways, we could gain insights into the potential roles of TMT in neurodegenerative diseases.

Upon examination of the transcriptomic data 168 h post-TMT administration, it is observed that 37 genes exhibited differential expression in the chemokine signaling pathway, accounting for 20% of the total genes in the pathway (Fig. 7). Notably, 2 genes (CXCL2, Rac1) were upregulated from 24 to 168 h, while 3 genes (STAT1, Hck, Nfkbia) showed upregulation from 48 to 168 h (Online Resource 1).

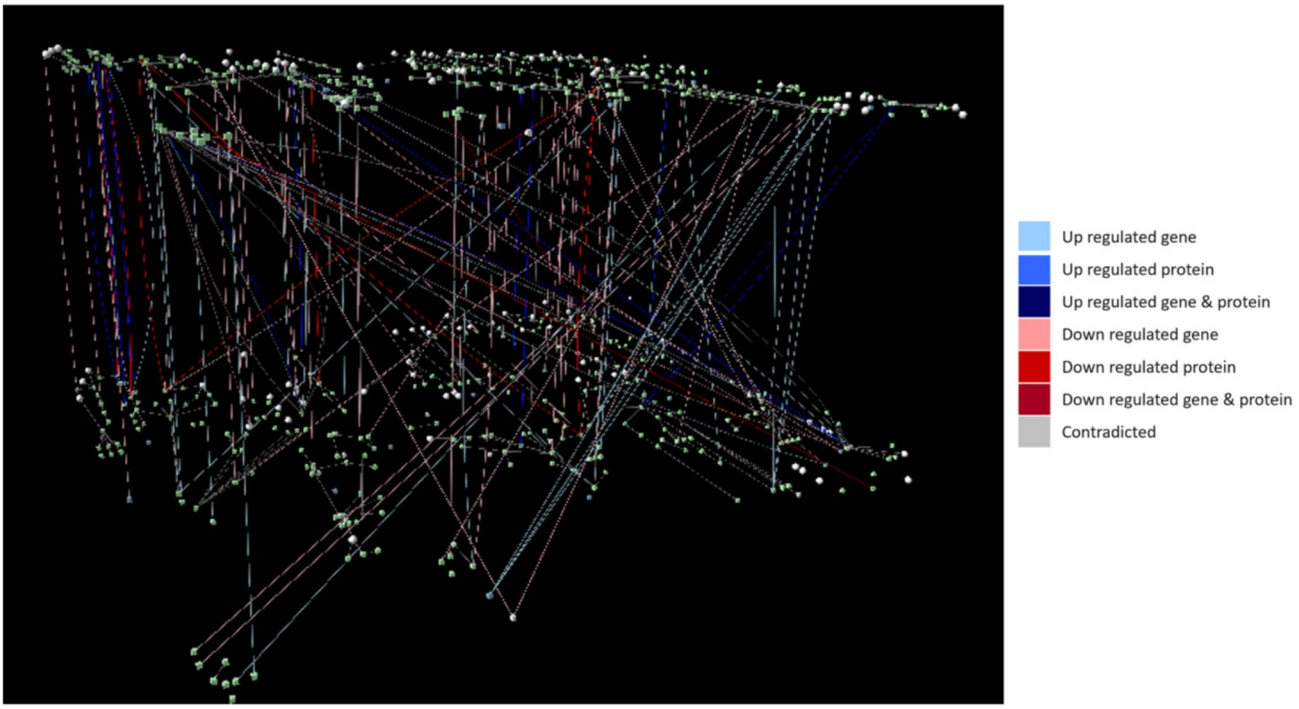


**Fig. 6** Alignment between transcriptomic (top layer) and proteomic (bottom layer) results in neurodegeneration pathways (rno05022) at 72 h after TMT administration. Light blue lines represent genes/proteins that are up regulated only in transcriptomics, blue lines represent genes/proteins that are up regulated only in proteomics, navy blue lines represent genes/proteins that are up regulated in both transcriptomics and proteomics, pink lines represent genes/proteins that are down regulated only in transcriptomics, red lines represent genes/proteins that are down regulated only in proteomics, dark red lines represent genes/proteins that are up regulated in both transcriptomics and proteomics, and grey lines represent contradicted regulation type (i.e. up regulated in one dataset and down regulated in the other)

In the apoptosis pathway, 42 genes, representing more than 30% of the total genes in the pathway, displayed differential expression (Fig. 8). Among these, 6 genes (Tnfrsf1a, Casp3, Ctsd, Mcl1, Tubal3, Gadd45a) were upregulated from 48 to 168 h (Online Resource 1).

In the TNF signaling pathway, 24 genes, comprising over 21% of the total genes in the pathway, exhibited differential expression (Fig. 9). Similarly, 6 genes (Tnfrsf1a, Mmp9, Icam1, Casp3, Bcl3, Nfkbia, Socs3) were upregulated from 48 to 168 h, and 1 gene (Traf3) showed upregulation from 12 to 168 h (Online Resource 1).

## IPA Analysis Match for Transcriptomics

Transcriptomic data from all time points was used in IPA Analysis Match. Following the filtration of the IPA Analysis Match results using hippocampus as the case tissue, a total of 16 datasets were discovered to align with our transcriptomic dataset with an overall similarity score exceeding 50%. Out of these, 11 datasets used in 5 studies were specifically focused on neurodegeneration in Alzheimer's disease (Online Resource 3). These studies address the Amyloid pathology (Benito et al. 2015; Cummings et al. 2015; Matarin et al. 2015) and Tau pathology (Matarin et al. 2015; Polito et al. 2014; Wes et al. 2014) in mouse models of Alzheimer's disease. Benito et al. (2015), Cummings et al. (2015), and Matarin et al. (2015) identified differentially expressed genes in models of cognitive decline and amyloid pathology, which align with our findings of synaptic dysfunction and neuro-axonal injury following TMT exposure (Benito et al. 2015; Cummings et al. 2015; Matarin et al. 2015). Similarly, Wes et al. (2014) reported neuroinflammation-driven transcriptional changes in tauopathy, mirroring the upregulation of inflammatory mediators and microglial activation markers in our dataset (Wes et al. 2014). Additionally, the overlap with Polito et al. (2014) suggests that autophagy and lysosomal dysfunction contribute to TMT-induced neuronal damage, consistent with our observed dysregulation of lysosomal and protein degradation pathways (Polito et al. 2014).

## Gene-Disease Associations (GDAs) with Alzheimer's Disease

After detecting Alzheimer's disease pathway among the top 15 affected KEGG pathways in both transcriptomics and proteomics, Open Targets and DISGENET plus services were utilized to acquire information on GDAs between

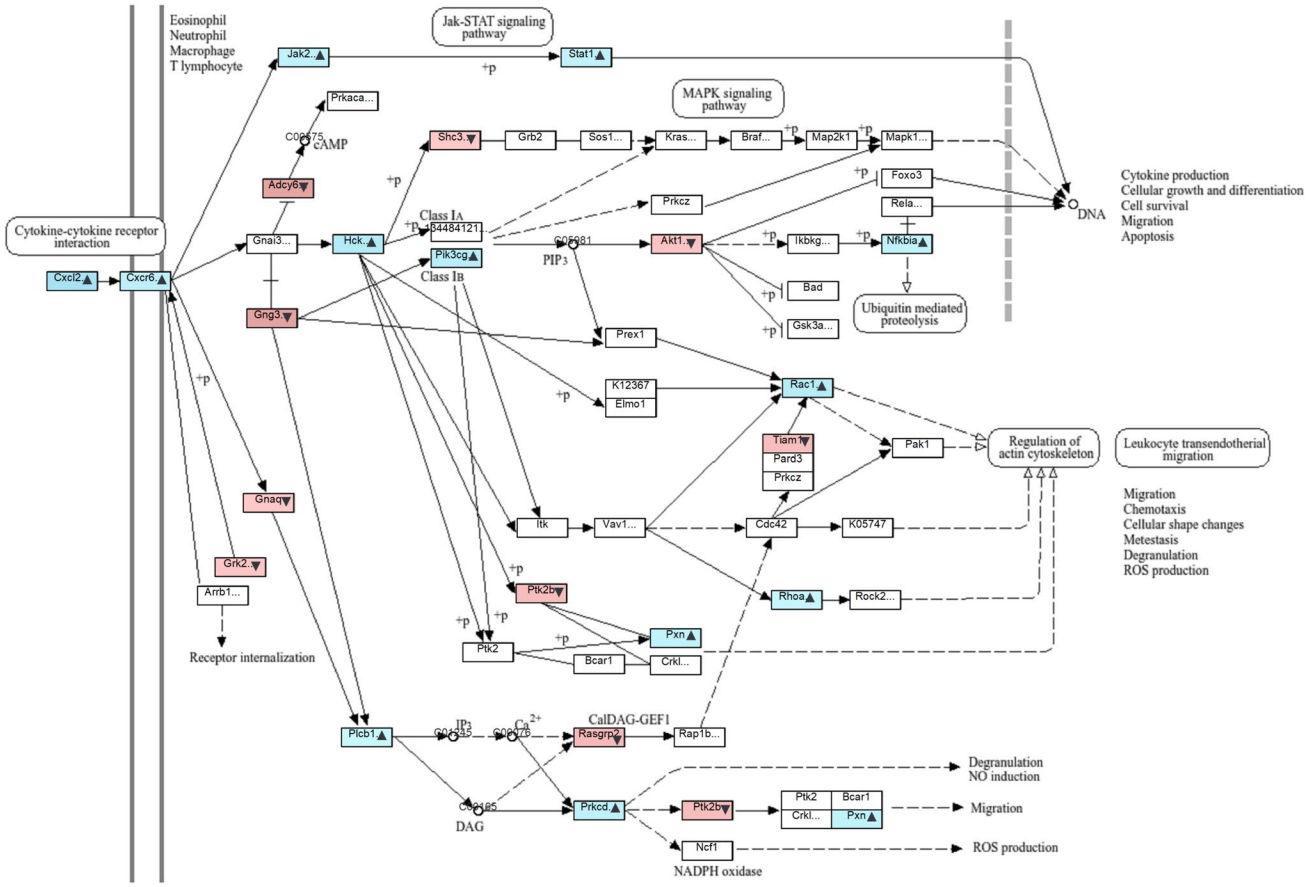


**Fig. 7** Differentially expressed genes in Chemokine Signaling Pathway (rno04062) using transcriptomic data at 168 h after TMT administration. Upregulated genes (*Q-value* < *0.05, Log*$_2$ *fold change* > *0.58*) are marked with blue and an upward-pointing triangle (▲) next to the gene name, while downregulated genes (*Q-value* < *0.05, Log*$_2$ *fold change* < *−0.58*) are marked with red and a downward-pointing triangle (▼) next to the gene name. Genes with no significant change are shown with an unfilled (white) box. Shading intensity represents the magnitude of log$_2$ fold change, with darker shading indicating larger expression changes. Chemokine signaling plays a key role in neuroinflammation, which is a hallmark of TMT-induced neurotoxicity

Alzheimer's disease (MONDO_0004975, C0002395) and differentially expressed genes/proteins after 168 h of TMT administration, which has the highest number of differentially expressed genes in transcriptomic data in Alzheimer's pathways (Fig. 5a). A total of 1163 GDAs were identified in transcriptomic data (Fig. 10), while 253 GDAs were discovered in proteomic data (Online Resource 4).

## Weighted Gene Co-expression Network Analysis (WGCNA) between DEGs and NfL Levels

To investigate the relationship between TMT-induced gene expression and NfL levels, differentially expressed genes from transcriptomic data were utilized in WGCNA analysis considering time, dose, and NfL levels. DEGs were categorized into nine modules (Fig. 11a), with the module eigengenes (MEs) of the black module, comprising 1,377 genes (approximately 23% of DEGs), demonstrating a strong positive correlation with dose, time, and NfL levels. The MEs of the green-yellow module, comprising 349 genes and approximately 6% of differentially expressed genes (DEGs), also exhibited a strong positive correlation with both dose and NfL levels (Fig. 11b).

In the black and green-yellow modules, gene significance for NfL exhibits a positive correlation with module membership, quantified at 0.8 and 0.62, respectively, both with significant *P*-values (Fig. 11c, Fig. 11d). This suggests that genes with high significance related to the trait are also the most connected within their respective module. Looking at driving genes (MM > 0.8 and GS > 0.5), we found 397 driving genes in the black module and 57 driving genes in the green-yellow module (Online Resources 8).

## Discussion

This research demonstrates how the usage of longitudinal omics data along with neuro-axonal damage marker can pinpoint the pathways and genes through which TMT induces

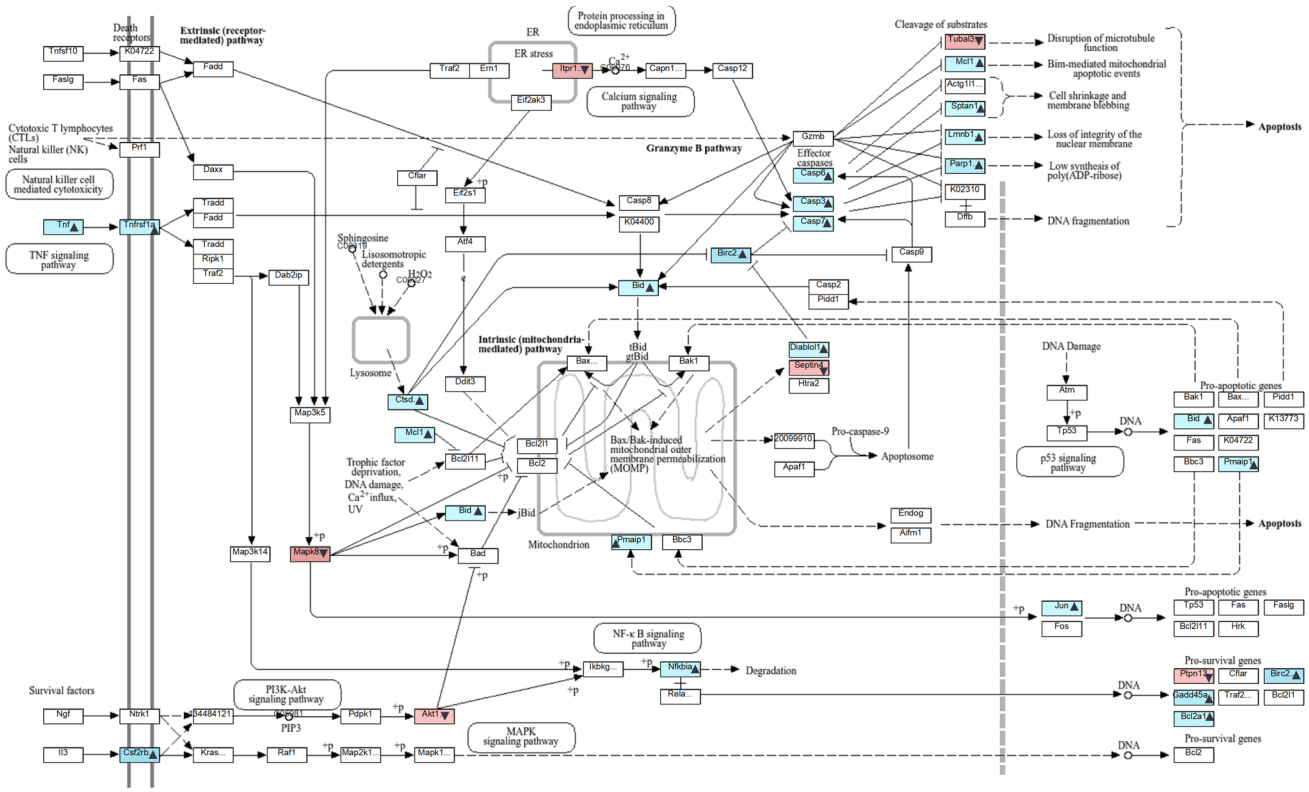


**Fig. 8** Differentially expressed genes in Apoptosis Pathway (rno04210) using transcriptomic data at 168 h after TMT administration. Upregulated genes (*Q-value* < *0.05, Log*$_2$ *fold change* > *0.58*) are marked with blue and an upward-pointing triangle (▲) next to the gene name, while downregulated genes (*Q-value* < *0.05, Log*$_2$ *fold change* < *−0.58*) are marked with red and a downward-pointing triangle (▼) next to the gene name. Genes with no significant change are shown with an unfilled (white) box. Shading intensity represents the magnitude of log$_2$ fold change, with darker shading indicating larger expression changes. Apoptotic processes are critical in TMT-induced neurodegeneration, mediating programmed cell death in affected hippocampal neurons

neurotoxicity and neuro-axonal damage and links that to various neurodegenerative conditions, including Alzheimer's disease.

The regulation of genes/proteins induced by TMT appears to happen gradually, with the peak occurring at 72 h and 168 h following administration (Fig. 2), which marks the time of neuro-axonal damage indicated by elevated NfL levels (Fig. 1). This gradual increase in response may be attributed to a dose-time dependent relationship, where the maximum response is observed during the later stages (Subashika et al. 2022) Consequently, it is crucial to measure gene/protein expression both in the early and late stages of neurotoxicant administration. Additionally, it is possible that certain transcription factors were activated during the early stages and required time to exert their influence on the expression of other genes. Alternatively, the neuro-axonal damage in some cells indicated by elevated NfL levels might have triggered differential gene/protein expression in other cells as well, increasing the number of differentially expressed genes and proteins at 72 h and 168 h after TMT administration.

In the TNF signaling pathway, several genes that contribute to neurodegeneration, such as TNFR1, MMP9, ICAM-1, and TRAF3 showed an increase in expression from 48 to 168 h after TMT administration in transcriptomic data (Fig. 9, Online Resource 1, Online Resource 2). One of these genes is Tnfrsf1a, which codes for TNFR1, the primary receptor for TNF. Neuronal TNF receptors perform fundamentally different roles in CNS pathology in vivo, with neuronal TNFR1 and IKKβ promoting microglial inflammation and neurotoxicity in demyelination (Orti-Casan et al. 2019; Papazian et al. 2021). Another upregulated gene is MMP9, which has dual effects. It promotes neurogenesis, angiogenesis, myelogenesis, and axonal growth, while also causing destructive effects such as apoptosis, disruption of the blood–brain barrier, and demyelination (Kaminari et al. 2018). Interestingly, MMP9 has been linked to Alzheimer's disease in the gene-disease association results of Open Targets and DISGENET plus (Online Resource 3). Furthermore, ICAM-1, whose transcript levels increased from 48 to 168 h after TMT administration, showed a corresponding rise in protein levels from 72 to 168 h after TMT

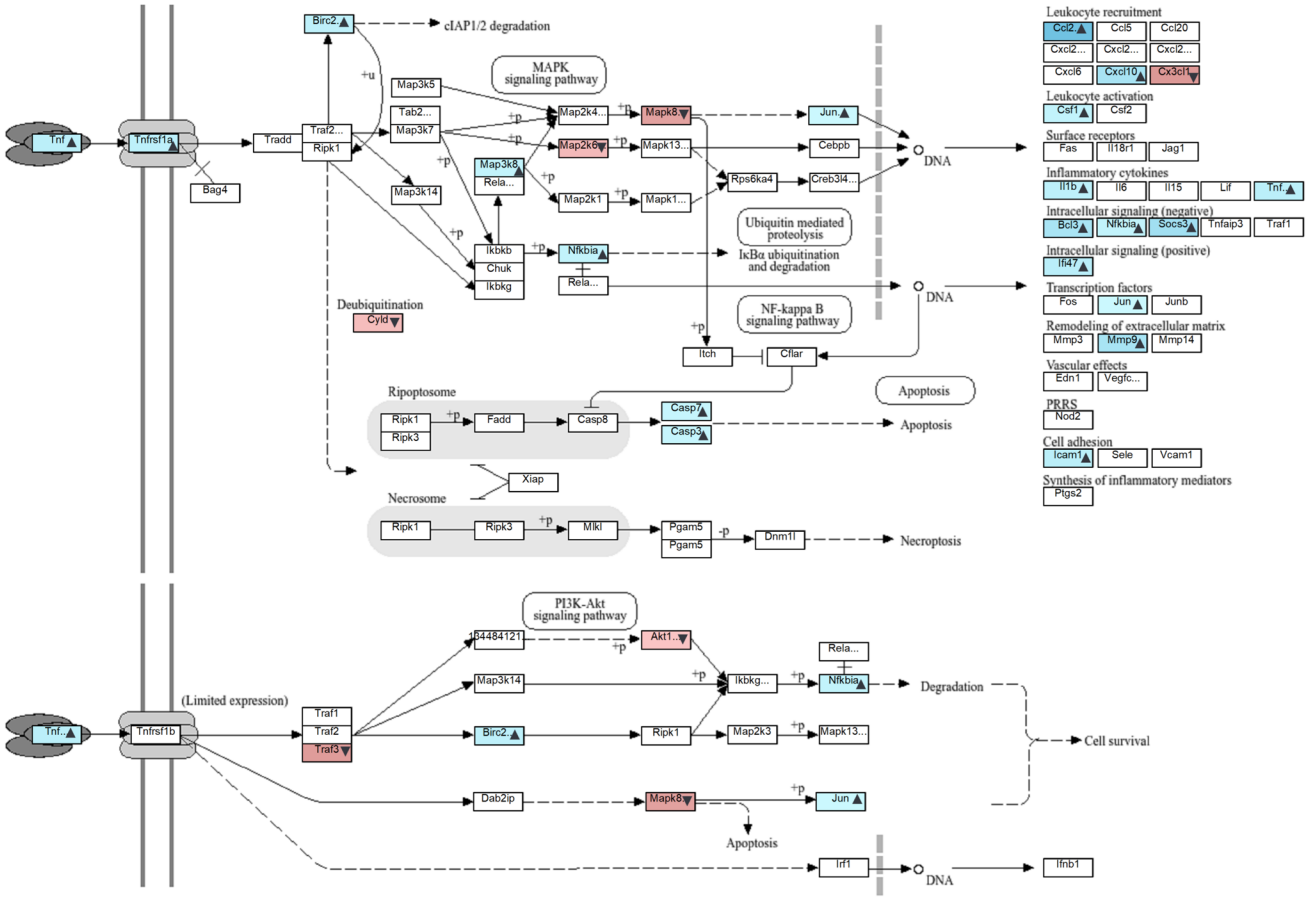


**Fig. 9** Differentially expressed genes in TNF Signaling Pathway (rno04668) using transcriptomic data at 168 h after TMT administration. Upregulated genes (*Q-value* < *0.05, Log*$_2$ *fold change* > *0.58*) are marked with blue and an upward-pointing triangle (▲) next to the gene name, while downregulated genes (*Q-value* < *0.05, Log*$_2$ *fold change* < *−0.58*) are marked with red and a downward-pointing triangle (▼) next to the gene name. Genes with no significant change are shown with an unfilled (white) box. Shading intensity represents the magnitude of log$_2$ fold change, with darker shading indicating larger expression changes. TNF signaling is a key driver of neuroinflammation and cell death in response to TMT toxicity, contributing to neurodegenerative processes

administration (Online Resource 1, 2). ICAM-1 contributes to neuroinflammation by inducing the expression of pro-inflammatory cytokines and chemokines (Walker et al. 2017). This gene was also associated with Alzheimer's disease in the gene-disease association results of DISGENET plus (Online Resource 4). In contrast, TRAF3 encoding for TNF Receptor-Associated Factor 3 exhibited a decrease in transcript levels from 12 to 168 h after TMT administration. TRAF3 is involved in regulating the calcineurin-NFAT pathway and NF-κB pathway, thereby preventing excessive inflammation (Wang et al. 2012). Therefore, the downregulation of TRAF3 may contribute to neurodegeneration. These results indicate that TMT-induced gene expression affects inflammation and apoptosis in different ways, leading to neurodegeneration like Alzheimer's disease.

Looking at the chemokine signaling pathway in transcriptomic data, various chemokines such as Cxcl10, Cxcl12, Cxcl14, and Cxcl16 exhibited upregulation from 24 to 168 h after TMT administration, indicating their involvement in the chemokine signaling pathway (Fig. 7, Online Resource 1). These chemokines are known to play a crucial role in neuroinflammation and have been found to be elevated in individuals with Alzheimer's disease (Li et al. 2023; Zuena et al. 2019). This correlation is further supported by the gene-disease association observed between Cxcl19 and Alzheimer's disease in the results from DISGENET plus (Online Resource 3). These results indicate the importance of neuroinflammation and chemokines in TMT-induced neurotoxicity.

In the apoptosis pathway, the Caspase-3 transcript shows an increase from 48 to 168 h post TMT administration (Fig. 8, Online Resource 1). Caspase-3 plays a crucial role in the apoptosis pathway that leads to neural cell death and is also involved in the TNF signaling pathway (Fig. 8, Fig. 9). Studies have shown its enrichment in the brains of Alzheimer's disease patients, particularly in the hippocampus

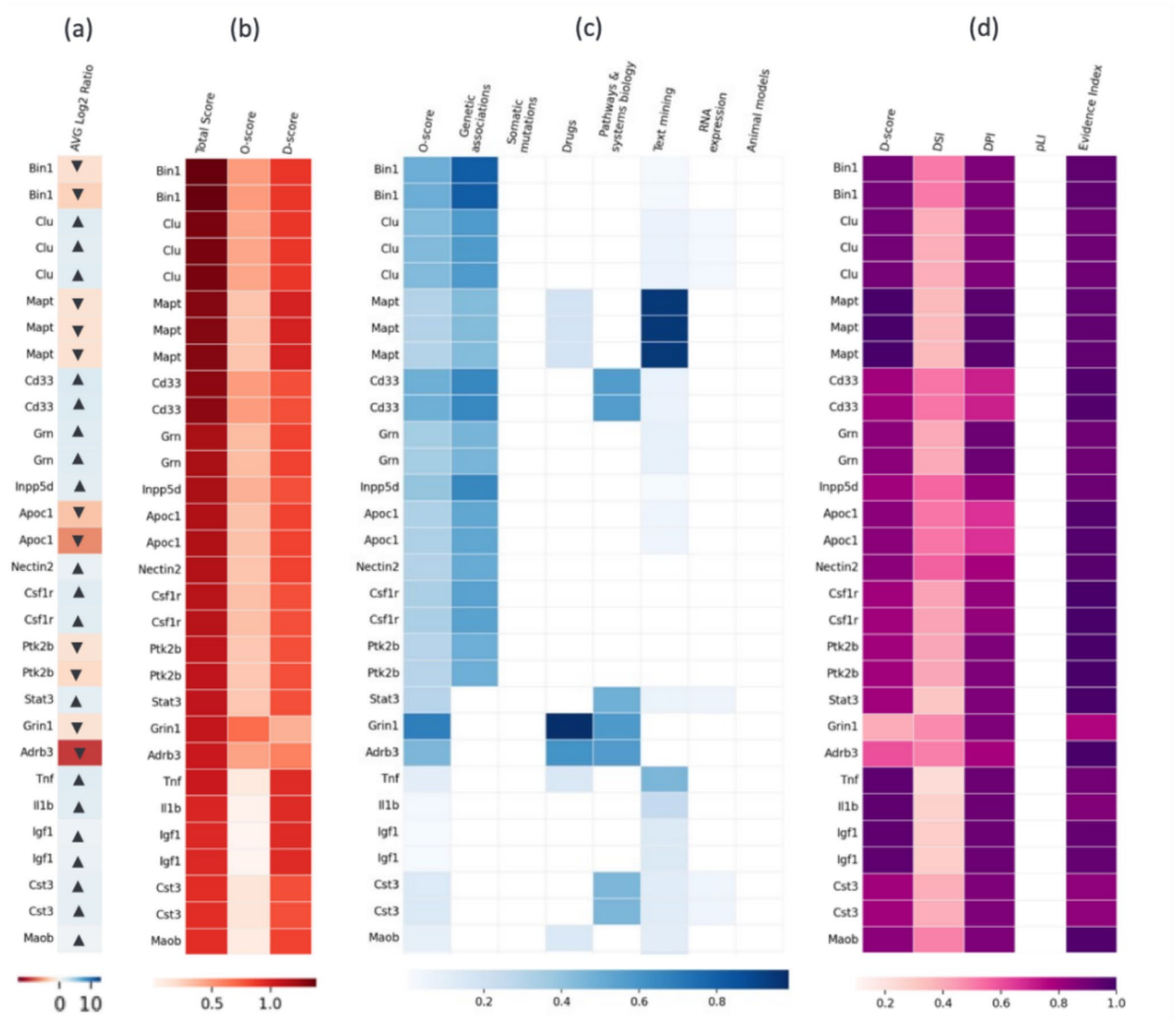


**Fig. 10** Top 30 Gene-Disease Association (GDA) scores between differentially expressed genes 168 h post TMT administration in transcriptomic data and Alzheimer's disease. (**a**) Expression heatmap of differentially expressed genes, where upregulated genes are marked with an upward-pointing triangle (▲) and downregulated genes with a downward-pointing triangle (▼). (**b**) Total GDA score from Open Targets and DISGENET combined. (**c**) Open Targets scores for individual genes. (**d**) DISGENET scores for individual genes. Shading intensity in (**b**), (**c**), and (**d**) represents the magnitude of the corresponding GDA scores, with darker shades indicating stronger associations

during the early stages of the disease (Louneva et al. 2008; Plociennik et al. 2015). Similarly, the PARP1 transcript is also upregulated within the same time frame. PARP1 acts as a primary sensor protein for DNA damage, and its upregulation after DNA damage results in mitochondrial dysfunction, increased oxidative stress, and NAD + depletion, which have been observed in various neurodegenerative diseases such as Parkinson's disease, Alzheimer's disease, Huntington's disease, and ALS (Thapa et al. 2021). The CTSD gene, responsible for encoding lysosomal cathepsin D, is also upregulated not only in transcriptomic data (from 24 to 168 h after TMT administration) but also in proteomic data (168 h after TMT administration) (Fig. 7, Online Resource 1, 2). Studies have reported its upregulation in the neocortex of Alzheimer's disease, leading to neurofibrillary degeneration (Chai et al. 2018). This finding is further supported by the GDA results linking Alzheimer's disease with CTSD (Online Resource 3). MCL1, which plays a role in the apoptotic/antiapoptotic balance of neurons (Mezache et al. 2015), is also upregulated from 48 to 168 h after TMT administration (Fig. 8,

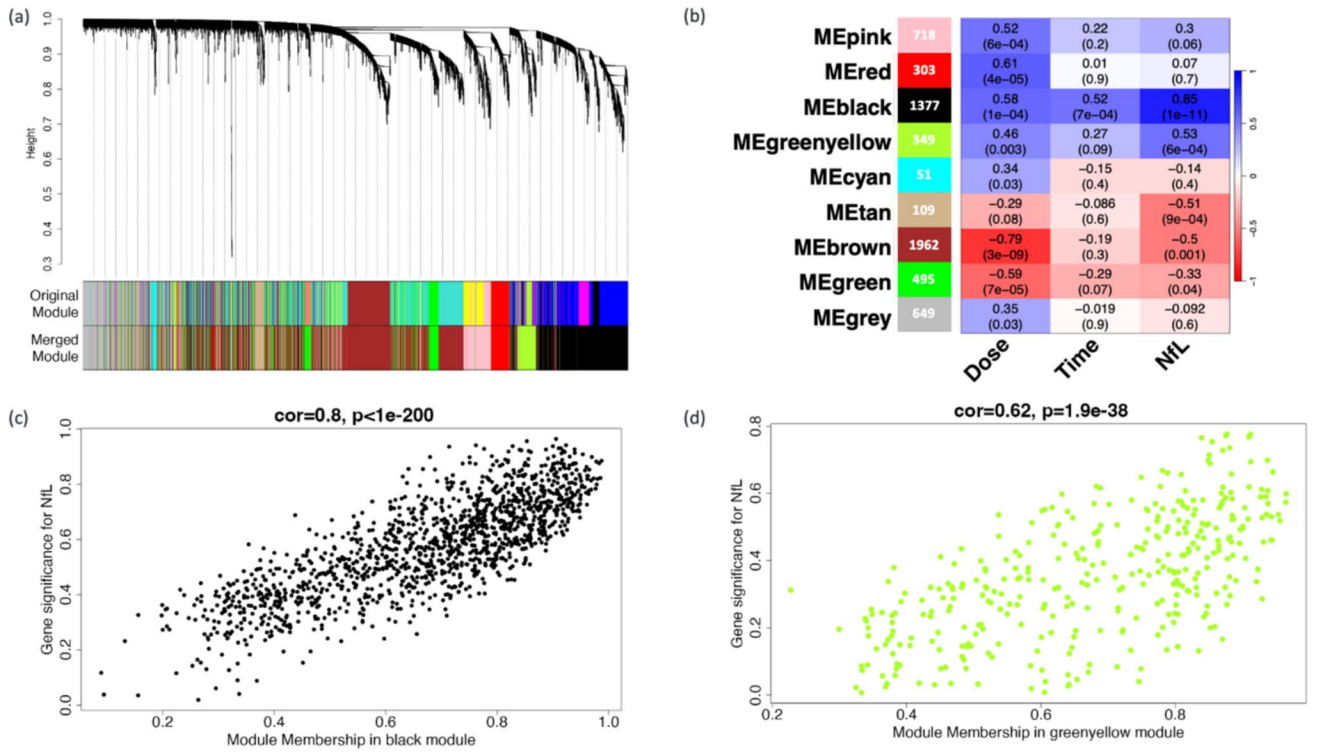


**Fig. 11** Weighted Gene Co-expression Network Analysis (WGCNA) between DEGs and NfL levels. (**a**) Gene dendrogram and module colors for original and merged modules. (**b**) Correlation heatmap between merged modules and dose, time, and NfL levels. Correlation coefficients ($R^2$ values) are written with *P*-values between parentheses. Positive correlation is represented in blue and negative correlation in red. The gene count for each module is indicated on the colored box of the module located to the left of the heatmap. (**c**-**d**) Scatterplot of the correlation between module membership and gene significance for NfL for genes in (c) black and (d) green-yellow modules. Correlation coefficients ($R^2$-values) and *P*-values are written on the top of plots

Online Resource 1) and has been associated with Alzheimer's disease in GDA results (Online Resource 4). These results highlight the role of various genes in the apoptosis pathway in the neural cell death caused by TMT administration and their associations with a couple of neurodegenerative diseases.

Beyond the chemokine signaling, TNF, and apoptosis pathways, several other mechanisms contribute to neuro-axonal damage, including synapse loss, autophagy, dysregulated calcium homeostasis, and impaired axonal guidance. The observed increase in plasma NfL levels suggests progressive neuronal injury, which can be linked to these molecular disruptions.

One of these genes is SNAP25, which encodes synaptosome-associated protein 25. This protein plays a role in regulating synaptic vesicle fusion and neurotransmitter release (Hoerder-Suabedissen et al. 2018). The transcriptomic data indicates that SNAP25 is downregulated from 48 to 168 h after TMT administration (Online Resource 4). This downregulation can potentially contribute to the loss of synapses, ultimately leading to neuro-axonal damage as indicated by NfL levels. Another gene, Lamp1, encodes for lysosomal membrane protein 1 and is involved in the autophagic pathway (Lattanzi et al. 2013). Both transcriptomic and proteomic data show an upregulation of Lamp1 at 168 h after TMT administration (Online Resource 4). Additionally, the upregulated CTSD gene in the chemokine signaling pathway (Online Resource 1) is also implicated in calcium signaling (Lattanzi et al. 2013). In fact, calcium homeostasis is another affected pathway, closely linked to axon integrity. Calcium signaling (rno04020) ranked among the top 15 disrupted pathways, with over 18% of its genes identified as DEGs. Notably, five key calcium-related genes (ATP2B2, Adrb2, Ryr1, Ppp3cc, Prkca) were downregulated from 48 to 168 h post-TMT administration (Online Resource 1). Disruptions in calcium homeostasis impair neuronal function, synaptic transmission, and cytoskeletal integrity, ultimately contributing to axonal degeneration and NfL elevation (Nagendran and Taylor 2019).

These findings suggest that synaptic dysfunction, autophagy dysregulation, and calcium disturbances are major pathways contributing to neuro-axonal damage, reflected by increased plasma NfL levels.

Another critical pathway in TMT-induced neurotoxicity is axon guidance (rno04360), essential for maintaining neuronal connectivity and regeneration. Within 48 h

post-TMT exposure, over 25% of its genes were differentially expressed, with eight key genes (Ntng2, Ntn3, Ppp3cc, Epha7, Ephb1, Pixna2, Sema6c, Wnt4, Camk2g) showing sustained downregulation from 48 to 168 h (Online Resource 1). Axon guidance disruption impairs neuronal repair and increases susceptibility to degeneration, likely contributing to elevated NfL levels as a marker of neuro-axonal damage.

Additionally, the neuroactive ligand-receptor interaction pathway (rno04080) is significantly affected by TMT exposure. At 48 h post-TMT administration, 12% of its genes were differentially expressed, with six genes (Chrm3, Kiss1r, Gabrg1, Pate10, Grin3b, Thrb) downregulated and seven genes (C3, C3ar1, Vgf, F2rl3, Calcb, Tspo) upregulated between 48 and 168 h (Online Resource 1). Among these, Gabrg1, which encodes the GABA-A receptor subunit gamma-1, plays a key role in GABAergic neurotransmission. Its downregulation could lead to altered inhibitory signaling, potentially contributing to excitotoxicity and neuronal damage, which in turn promotes axonal injury and increased NfL release (Cheng et al. 2017). Similarly, the downregulation of Grin3b, which encodes NMDA receptor subunit 3B, may impair glutamatergic signaling and synaptic plasticity, further weakening neuronal resilience to toxic insults (Kirtay et al. 2021).

Notably, Prkca and Gabrg1 are also part of the GABAergic synapse pathway (rno04727), reinforcing the role of inhibitory neurotransmission in TMT-induced neurotoxicity.

Collectively, these findings suggest that disruptions in GABAergic and glutamatergic signaling, combined with calcium homeostasis imbalance, autophagy dysregulation, and impaired axonal guidance, contribute to neuro-axonal damage following TMT exposure. The resulting synaptic dysfunction, neuronal stress, and impaired repair mechanisms likely drive the elevation of plasma NfL levels, reinforcing its role as a biomarker of axonal injury.

At 72 h after TMT administration, two genes in neurodegenerative disease pathways showed identical regulation patterns in both transcriptome and proteomic data (Fig. 6, Online Resource 4, Online Resource 7). Psmb3, which is elevated in both transcriptome and proteomic data, is an essential component of the ubiquitin–proteasome system (UPS), which aids in protein quality control and degradation pathways that are frequently disturbed in many neurodegenerative illnesses. Its overexpression may increase proteasome activity, resulting in faster destruction of damaged or misfolded proteins. Nonetheless, excessive degradation or dysregulated proteasome function caused by increased Psmb3 levels may also result in a cellular proteostasis imbalance, thereby aggravating cellular dysfunction or contributing to disease progression (Ding and Zhu 2018). Tubb4a, on the other hand, is downregulated across both transcriptome and proteomic datasets. Tubb4a is an important component of microtubules, which are responsible for cellular structure, intracellular transport, and division. Tubb4a mutations have been associated with hypomyelination and other neurological diseases, showing that it plays an important role in neuronal development (Duncan et al. 2017). It can also affect microtubule dynamics during stressful situations, making neurons more vulnerable (Liang et al. 2024).

In addition to the genes previously mentioned, over 1700 proteins exhibited significant changes exclusively in the proteomic data with no change in transcriptomic data. Among them, 11 proteins showed significant alterations between 72 to 168 h following TMT administration and displayed associations with Alzheimer's disease. These findings could be attributed to post-translational modifications impacting protein levels without affecting transcription. Among these 11 genes, 9 (APP, APLP1, APLP2, Hsd17b12, PLD3, PCOLCE, FABP5, ATP6AP2) were upregulated and 3 (RELN, PCP4, Ppp1r14c) were downregulated from 72 to 168 h post TMT administration. Upregulation of APP (Amyloid Precursor Protein) was reported to cause increased production of amyloid beta (Aβ) peptides, especially Aβ42, which are prone to aggregation and form amyloid plaques characteristic of Alzheimer's disease. It has been associated with increased production of reactive oxygen species (ROS), which can cause oxidative stress and contribute to neurodegeneration. (Nithianandam et al. 2023; Zhou et al. 2011). APLP1 (Amyloid Precursor-Like Protein 1) and APLP2 (Amyloid Precursor-Like Protein 2) have been reported to be related to APP (Arvidsson et al. 2008). PLD3 upregulation has also been associated with lysosomal dysfunction and β-amyloid plaque formation (Nackenoff et al. 2021). ATP6AP2 encodes an accessory protein of the vacuolar $H^+$-ATPase (V-ATPase) complex, which is crucial for lysosomal acidification and protein degradation. These results show that TMT-induced neurotoxicity can affect the proteins related to β-amyloid plaques formation in a post-translational manner, which then leads to neurodegeneration in a manner similar to Alzheimer's disease. Furthermore, RELN, which is downregulated between 72 and 168 h after TMT administration, encodes a glycoprotein for the extracellular matrix that is essential for appropriate cortical layering in the brain and cerebellum during neurodevelopment. It contributes to the pathophysiology of Alzheimer's dementia (AD) by being a component of the apolipoprotein E (apoE) biochemical pathway (Seripa et al. 2008).

The examination of the relationship between TMT-induced gene expression and NfL levels, employing WGCNA on DEGs derived from transcriptomic data, revealed 1,377 genes in the black module that demonstrated a strong correlation with NfL, dose, and time, as well as 349 genes in the green-yellow module that correlated significantly with NfL levels. This represents about 29% of the differentially expressed genes in TMT-treated rats (Fig. 11a, Fig. 11b). The positive correlation values between module

membership and gene significance for NfL in the black (Fig. 11c) and green-yellow (Fig. 11d) modules highlight the potential of these genes in targeting NfL. In these modules, the driving genes were identified as 397 in the black module and 57 in the green-yellow module, with thresholds set at MM > 0.8 and GS > 0.5. This represents roughly 6% of the total differentially expressed genes (DEGs). Among the 454 genes analyzed, 450 were found to have associations with Alzheimer's disease.

Furthermore, we identified Hck from the chemokine signaling pathway (Fig. 7), Mcl and Ctsd from the apoptosis pathways (Fig. 8), and Tnfrsfla from both apoptosis and TNF signaling pathways, all of which exhibited upregulation from 48 to 168 h post-TMT administration. The findings demonstrate a correlation between TMT-induced gene expression and neuro-axonal damage, as evidenced by NfL levels, and further substantiate the link between TMT-induced neurotoxicity and Alzheimer's disease.

The results also point to several areas for further study in the fields of neurotoxicity and neurodegeneration. A list of possible targets for therapeutic approaches is suggested by the 450 driving genes in the black and green-yellow modules that exhibit GDAs with Alzheimer's disease. Specifically, the identified driving genes in the TNF signaling pathways (Tnfrsfla), chemokine signaling (Hck), and apoptosis (Ctsd, Mcl) provide therapeutic targets for neuroprotective measures. Additional functional studies are necessary to confirm the significance of identified molecular targets and pathways in human tissue samples or cell models, as well as to validate potential therapeutic targets. Furthermore, examining cell type-specific responses to TMT administration using techniques such as single-cell sequencing may provide comprehensive insights into the mechanisms of neurotoxicity.

## Conclusions

This study presents a comprehensive investigation into the harmful effects of TMT on the central nervous system by analyzing transcriptomic and proteomic data, to understand the time-dependent TMT-induced neurotoxicity with relation to neuro-axonal damage marked by elevated NfL levels.

Neuro-axonal damage that seems to occur at 72 h and 168 h after TMT administration is induced by a number of differentially expressed genes/proteins starting from 48 h after TMT administration. More than ten genes were found to be differentially expressed from 48 h after TMT administration in different neurodegenerative diseases related pathways, including chemokine signaling, apoptosis, TNF pathway, and calcium homeostasis. Alzheimer's disease and neurodegenerative disease pathways were among the top 15 affected pathways in both transcriptomics and proteomics. In addition, 11 Alzheimer's disease-related genes were found to have significant changes only in proteomics, indicating the possibility of post-translational modification. The association between TMT-induced gene regulation and Alzheimer's disease is further confirmed through 9 studies confirmed to be an Analysis Match by IPA and more than a thousand gene-disease associations between Alzheimer's and transcriptomic data and more than 200 associations with proteomic data. WGCNA between DEGs and NfL levels further emphasizes the relationship between TMT-induced gene expression and neuro-axonal damage marked by elevated NfL levels. 454 driving genes were identified, and 450 of them were found to have GDAs with Alzheimer's disease.

This research emphasizes the importance of employing a longitudinal omics approach, along with pathway enrichment analysis, analysis match, gene-disease association analysis, and neuro-axonal damage biomarker analysis, to unravel the pathways and molecules involved in the time-based neurotoxicant-induced neurodegeneration.

**Supplementary Information** The online version contains supplementary material available at https://doi.org/10.1007/s12640-025-00737-3.

**Acknowledgements** The authors would like to thank Kazuko Watanabe and Kazumi Ohuchi of the DMPK&modeling, Takeda Pharmaceutical Company Ltd. for supporting proteomics assay and biomarker measurements. We also thank Naohiro Narita for his help planning animal and omics studies. And finally, we appreciate the effort of the research members at Takeda Pharmaceutical Company Ltd. in their experimental and technical contributions.

**Author Contributions** Douaa Zakaria: Substantial contributions to conduct multi-omics analysis and interpretation of data for the work.; drafting the work manuscript.

Tomoki Yamashita: Proposal of multi-omics analysis, interpretation of data for the work; review the manuscript.

Yohei Kosugi: Substantial contributions to the conception and design of the work; interpretation of data for the work; review the manuscript; final approval of the version to be published.

**Funding** The study used the internal budget of Takeda Pharmaceutical Company Limited.

**Data Availability** No datasets were generated or analysed during the current study.

## Declarations

**Competing Interests** The authors declare no competing interests.

**Ethics** The animal studies were performed in facilities accredited by the Association for Assessment and Accreditation of Laboratory Animal Care International (AAALAC) according to the Guide for the Care and Use of Laboratory Animals.

## References

Arvidsson Y, Andersson E, Bergstrom A, Andersson MK, Altiparmak G, Illerskog A-C, Ahlman H, Lamazhapova D, Nilsson O (2008) Amyloid precursor-like protein 1 is differentially upregulated in neuroendocrine tumours of the gastrointestinal tract. Endocr Relat Cancer 15(2):569–581. https://doi.org/10.1677/erc-07-0145

Benito E, Urbanke H, Ramachandran B, Barth J, Halder R, Awasthi A, Jain G, Capece V, Burkhardt S, Navarro-Sala M, Nagarajan S, Schütz AL, Johnsen SA, Bonn S, Lührmann R, Dean C, Fischer A (2015) HDAC inhibitor-dependent transcriptome and memory reinstatement in cognitive decline models. J Clin Investig 125(9):3572–3584. https://doi.org/10.1172/JCI79942

Ceccariglia S, D'Altocolle A, Del Fa A, Pizzolante F, Caccia E, Michetti F, Gangitano C (2011) Cathepsin D plays a crucial role in the trimethyltin-induced hippocampal neurodegeneration process. Neuroscience 174:160–170. https://doi.org/10.1016/j.neuroscience.2010.11.024

Chai YL, Chong JR, Weng J, Howlett D, Halsey A, Lee JH, Attems J, Aarsland D, Francis PT, Chen CP, Lai MKP (2018) Lysosomal cathepsin D is upregulated in alzheimer's disease neocortex and may be a marker for neurofibrillary degeneration. Brain Pathol 29(1):63–74. https://doi.org/10.1111/bpa.12631

Chang LW, Wenger GR, McMillan DE, Dyer RS (1983) Species and strain comparison of acute neurotoxic effects of trimethyltin in mice and rats. Neurobehav Toxicol Teratol 5(3):337–350

Cheng Q, Wang YX, Yu J, Yi S (2017) Critical signaling pathways during Wallerian degeneration of peripheral nerve. Neural Regen Res 12(6):995–1002. https://doi.org/10.4103/1673-5374.208596

Cokelaer T, Pultz D, Harder LM, Serra-Musach J, Saez-Rodriguez J (2013) BioServices: a common python package to access biological web services programmatically. Bioinformatics 29(24):3241–3242. https://doi.org/10.1093/bioinformatics/btt547

Corvino V, Geloso MC, Cavallo V, Guadagni E, Passalacqua R, Florenzano F, Giannetti S, Molinari M, Michetti F (2005) Enhanced neurogenesis during trimethyltin-induced neurodegeneration in the hippocampus of the adult rat. Brain Res Bull 65(6):471–477. https://doi.org/10.1016/j.brainresbull.2005.02.031

Cummings DM, Liu W, Portelius E, Bayram S, Yasvoina M, Ho SH, Smits H, Ali SS, Steinberg R, Pegasiou CM, James OT, Matarin M, Richardson JC, Zetterberg H, Blennow K, Hardy JA, Salih DA, Edwards FA (2015) First effects of rising amyloid-β in transgenic mouse brain: synaptic transmission and gene expression. Brain: J Neurol 138(Pt 7):1992–2004. https://doi.org/10.1093/brain/awv127

Ding Q, Zhu H (2018) Upregulation of PSMB8 and cathepsins in the human brains of dementia with Lewy bodies. Neurosci Lett 678:131–137. https://doi.org/10.1016/j.neulet.2018.05.022

Duncan ID, Bugiani M, Radcliff AB, Moran JJ, Lopez-Anido C, Duong P, August BK, Wolf NI, van der Knaap MS, Svaren J (2017) A mutation in the Tubb4a gene leads to microtubule accumulation with hypomyelination and demyelination. Ann Neurol 81(5):690–702. https://doi.org/10.1002/ana.24930

Edalatmanesh MA, Hosseini M, Ghasemi S, Golestani S, Sadeghnia HR, Mousavi SM, Vafaee F (2015) Valproic acid-mediated inhibition of trimethyltin-induced deficits in memory and learning in the rat does not directly depend on its anti-oxidant properties. Irish J Med Sci (1971-) 185(1):75–84. https://doi.org/10.1007/s11845-014-1224-y

Gaetani L, Blennow K, Calabresi P, Di Filippo M, Parnetti L, Zetterberg H (2019) Neurofilament light chain as a biomarker in neurological disorders. J Neurol Neurosurg Psychiatry 90:870–881

Geloso MC, Corvino V, Michetti F (2011) Trimethyltin-induced hippocampal degeneration as a tool to investigate neurodegenerative processes. Neurochem Int 58(7):729–738. https://doi.org/10.1016/j.neuint.2011.03.009

Hoerder-Suabedissen A, Korrell KV, Hayashi S, Jeans A, Ramirez DM, Grant E, Christian HC, Kavalali ET, Wilson MC, Molnár Z (2018) Cell-specific loss of SNAP25 from cortical projection neurons allows normal development but causes subsequent neurodegeneration. Cereb Cortex 29(5):2148–2159. https://doi.org/10.1093/cercor/bhy127

Hou J, Cui C, Kim S, Sung C, Choi C (2018) Ginsenoside F1 suppresses astrocytic senescence-associated secretory phenotype. Chem Biol Interact 283:75–83. https://doi.org/10.1016/j.cbi.2018.02.002

Imam SZ, He Z, Cuevas E, Rosas-Hernandez H, Lantz SM, Sarkar S, Raymick J, Robinson B, Hanig JP, Herr D, MacMillan D, Smith A, Liachenko S, Ferguson S, O'Callaghan J, Miller D, Somps C, Pardo ID, Slikker W Jr, Paule MG (2017) Changes in the metabolome and microrna levels in biological fluids might represent biomarkers of neurotoxicity: a trimethyltin study. Exp Biol Med 243(3):228–236. https://doi.org/10.1177/1535370217739859

Kaminari A, Tsilibary EC, Tzinia A (2018) A new perspective in utilizing MMP-9 as a therapeutic target for alzheimer's disease and type 2 diabetes mellitus. J Alzheimer's Disease 64(1):1–16. https://doi.org/10.3233/jad-180035

Kaur S, Chhabra R, Nehru B (2013) Ginkgo biloba extract attenuates hippocampal neuronal loss and cognitive dysfunction resulting from trimethyltin in mice. Phytomedicine 20(2):178–186. https://doi.org/10.1016/j.phymed.2012.10.003

Khalil M, Teunissen CE, Otto M, Piehl F, Sormani MP, Gattringer T, Barro C, Kappos L, Comabella M, Fazekas F et al (2018) Neurofilaments as biomarkers in neurological disorders. Nat Rev Neurol 14:577–589

Kirtay M, Sell J, Marx C, Haselmann H, Ceanga M, Zhou ZW, Rahmati V, Kirkpatrick J, Buder K, Grigaravicius P, Ori A, Geis C, Wang ZQ (2021) ATR regulates neuronal activity by modulating presynaptic firing. Nat Commun 12(1):4067. https://doi.org/10.1038/s41467-021-24217-2

Kuhle J, Barro C, Andreasson U, Derfuss T, Lindberg R, Sandelius A, Liman V, Norgren N, Blennow K, Zetterberg H (2016) Comparison of three analytical platforms for quantification of the neurofilament light chain in blood samples: ELISA, electrochemiluminescence immunoassay and simoa. Clin Chem Lab Med 54:1655–1661

Kurkowska-Jastrzebska I, Joniec I, Zaremba M, Fiedorowicz A, Czlonkowska A, Oderfeld-Nowak B (2007) Anti-myelin basic protein T cells protect hippocampal neurons against trimethyltin-induced damage. NeuroReport 18(5):425–429. https://doi.org/10.1097/wnr.0b013e3280586777

Langfelder P, Horvath S (2008) WGCNA: an R package for weighted correlation network analysis. BMC Bioinform 9:559. https://doi.org/10.1186/1471-2105-9-559

Lattanzi W, Corvino V, Di Maria V, Michetti F, Geloso MC (2013) Gene expression profiling as a tool to investigate the molecular machinery activated during hippocampal neurodegeneration induced by trimethyltin (TMT) administration. Int J Mol Sci 14(8):16817–16835. https://doi.org/10.3390/ijms140816817

Lee S, Yang M, Kim J, Kang S, Kim J, Kim J-C, Jung C, Shin T, Kim S-H, Moon C (2016) Trimethyltin-induced hippocampal neurodegeneration: a mechanism-based review. Brain Res Bull 125:187–199. https://doi.org/10.1016/j.brainresbull.2016.07.010

Lelong S, Zhou X, Afrasiabi C, Qian Z, Cano MA, Tsueng G, Xin J, Mullen J, Yao Y, Avila R, Taylor G, Su AI, Wu C (2022) Biothings SDK: a toolkit for building high-performance data apis in biomedical research. Bioinformatics 38(7):2077–2079. https://doi.org/10.1093/bioinformatics/btac017

Li X, Zhang D-F, Bi R, Tan L-W, Chen X, Xu M, Yao Y-G (2023) Convergent transcriptomic and genomic evidence supporting a dysregulation of CXCL16 and CCL5 in alzheimer's disease. Alzheimer's Res Therapy 15(1). https://doi.org/10.1186/s13195-022-01159-5

Liang X, Gong M, Wang Z et al (2024) LncRNA TubAR complexes with TUBB4A and TUBA1A to promote microtubule assembly and maintain myelination. Cell Discov 10:54. https://doi.org/10.1038/s41421-024-00667-y

Little AR, Benkovic SA, Miller DB, O'Callaghan JP (2002) Chemically induced neuronal damage and gliosis: Enhanced expression of the proinflammatory chemokine, monocyte chemoattractant protein (MCP)-1, without a corresponding increase in proinflammatory cytokines. Neuroscience 115(1):307–320. https://doi.org/10.1016/s0306-4522(02)00359-7

Louneva N, Cohen JW, Han L-Y, Talbot K, Wilson RS, Bennett DA, Trojanowski JQ, Arnold SE (2008) Caspase-3 is enriched in postsynaptic densities and increased in alzheimer's disease. Am J Pathol 173(5):1488–1495. https://doi.org/10.2353/ajpath.2008.080434

Matarin M, Salih DA, Yasvoina M, Cummings DM, Guelfi S, Liu W, Nahaboo Solim MA, Moens TG, Paublete RM, Ali SS, Perona M, Desai R, Smith KJ, Latcham J, Fulleylove M, Richardson JC, Hardy J, Edwards FA (2015) A genome-wide gene-expression analysis and database in transgenic mice during development of amyloid or tau pathology. Cell Rep 10(4):633–644. https://doi.org/10.1016/j.celrep.2014.12.041

Mezache L, Mikhail M, Garofalo M, Nuovo GJ (2015) Reduced Mir-512 and the elevated expression of its targets cFLIP and MCL1 localize to neurons with hyperphosphorylated tau protein in alzheimer disease. Appl Immunohistochem Mol Morphol 23(9):615–623. https://doi.org/10.1097/pai.0000000000000147

Nackenoff AG, Hohman TJ, Neuner SM, Akers CS, Weitzel NC, Shostak A, Ferguson SM, Mobley B, Bennett DA, Schneider JA, Jefferson AL, Kaczorowski CC, Schrag MS (2021) PLD3 is a neuronal lysosomal phospholipase D associated with β-amyloid plaques and cognitive function in alzheimer's disease. PLOS Genet 17(4). https://doi.org/10.1371/journal.pgen.1009406

Nagendran T, Taylor AM (2019) Unique axon-to-soma signaling pathways mediate dendritic spine loss and hyper-excitability post-axotomy. Front Cell Neurosci 13:431. https://doi.org/10.3389/fncel.2019.00431

Nishida K, Maruyama J, Kaizu K, Takahashi K, Yugi K (2024) Transomics2cytoscape: an automated software for interpretable 2.5-dimensional visualization of trans-OMIC Networks. Npj Syst Biol Appl 10(1). https://doi.org/10.1038/S31540-024-00342-8

Nithianandam V, Bukhari H, Leventhal MJ, Battaglia RA, Dong X, Fraenkel E, Feany MB (2023) Integrative analysis reveals a conserved role for the amyloid precursor protein in proteostasis during aging. Nat Comm 14(1). https://doi.org/10.1038/s41467-023-42822-1

Ochoa D, Hercules A, Carmona M, Suveges D, Baker J, Malangone C, Lopez I, Miranda A, Cruz-Castillo C, Fumis L, Bernal-Llinares M, Tsukanov K, Cornu H, Tsirigos K, Razuvayevskaya O, Buniello A, Schwartzentruber J, Karim M, Ariano B, … McDonagh EM (2022) The next-generation open targets platform: Reimagined, redesigned, rebuilt. Nucleic Acids Res 51(D1). https://doi.org/10.1093/nar/gkac1046

Ogata K, Sumida K, Miyata K, Kushida M, Kuwamura M, Yamate J (2014) Circulating mir-9* and mir-384-5p as potential indicators for trimethyltin-induced neurotoxicity. Toxicol Pathol 43(2):198–208. https://doi.org/10.1177/0192623314530533

Orti-Casan N, Wu Y, Naudé PJ, De Deyn PP, Zuhorn IS, Eisel UL (2019) Targeting TNFR2 as a novel therapeutic strategy for alzheimer's disease. Front Neurosci 13. https://doi.org/10.3389/fnins.2019.00049

Papazian I, Tsoukala E, Boutou A et al (2021) Fundamentally different roles of neuronal TNF receptors in CNS pathology: TNFR1 and IKKβ promote microglial responses and tissue injury in demyelination while TNFR2 protects against excitotoxicity in mice. J Neuroinflammation 18:222. https://doi.org/10.1186/s12974-021-02200-4

Piñero J, Ramírez-Anguita JM, Saüch-Pitarch J, Ronzano F, Centeno E, Sanz F, Furlong LI (2019) The DisGeNET knowledge platform for disease genomics: 2019 update. Nucleic Acids Res. https://doi.org/10.1093/nar/gkz1021

Plociennik A, Prendecki M, Zuba E, Siudzinski M, Dorszewska J (2015) Activated caspase-3 and neurodegeneration and synaptic plasticity in alzheimer's disease. Adv Alzheimer's Disease 04(03):63–77. https://doi.org/10.4236/aad.2015.43007

Polito VA, Li H, Martini-Stoica H, Wang B, Yang L, Xu Y, Swartzlander DB, Palmieri M, di Ronza A, Lee VM, Sardiello M, Ballabio A, Zheng H (2014) Selective clearance of aberrant tau proteins and rescue of neurotoxicity by transcription factor EB. EMBO Mol Med 6(9):1142–1160. https://doi.org/10.15252/emmm.201303671

Sano T, Masuda Y, Yasuno H, Shinozawa T, Watanabe T, Kakehi M (2021) Blood neurofilament light chain as a potential biomarker for central and peripheral nervous toxicity in rats. Toxicol Sci 185(1):10–18. https://doi.org/10.1093/toxsci/kfab122

Schvartz D, González-Ruiz V, Walter N, Antinori P, Jeanneret F, Tonoli D, Boccard J, Zurich M-G, Rudaz S, Monnet-Tschudi F, Sandström J, Sanchez J-C (2019) Protein pathway analysis to study development-dependent effects of acute and repeated trimethyltin (TMT) treatments in 3D rat brain cell cultures. Toxicol in Vitro 60:281–292. https://doi.org/10.1016/j.tiv.2019.05.020

Seripa D, Matera MG, Franceschi M, Daniele A, Bizzarro A, Rinaldi M, Panza F, Fazio VM, Gravina C, D'Onofrio G, Solfrizzi V, Masullo C, Pilotto A (2008) The reln locus in alzheimer's disease. J Alzheimer's Disease 14(3):335–344. https://doi.org/10.3233/jad-2008-14308

Shin E-J, Suh SK, Lim YK, Jhoo W-K, Hjelle OP, Ottersen OP, Shin CY, Ko KH, Kim W-K, Kim DS, Chun W, Ali S, Kim H-C (2005) Ascorbate attenuates trimethyltin-induced oxidative burden and neuronal degeneration in the rat hippocampus by maintaining glutathione homeostasis. Neuroscience 133(3):715–727. https://doi.org/10.1016/j.neuroscience.2005.02.030

Subashika G, Daniel A, Stoppini L, Deplancke B, Adrien R (2022) Neuro-toxicogenomic mapping of TMT induced neurotoxicity using human minibrain reveals associated adverse outcome events. Preprint at https://www.biorxiv.org/content/https://doi.org/10.1101/2022.01.21.477206v1.abstract

Thapa K, Khan H, Sharma U, Grewal AK, Singh TG (2021) Poly (ADP-ribose) polymerase-1 as a promising drug target for neurodegenerative diseases. Life Sci 267:118975. https://doi.org/10.1016/j.lfs.2020.118975

Vogel C, Marcotte EM (2012) Insights into the regulation of protein abundance from proteomic and transcriptomic analyses. Nat Rev Genet 13(4):227–232. https://doi.org/10.1038/nrg3185

Walker DG, Lue L-F, Tang TM, Adler CH, Caviness JN, Sabbagh MN, Serrano GE, Sue LI, Beach TG (2017) Changes in CD200 and intercellular adhesion molecule-1 (ICAM-1) levels in brains

of Lewy body disorder cases are associated with amounts of alzheimer's pathology not α-synuclein pathology. Neurobiol Aging 54:175–186. https://doi.org/10.1016/j.neurobiolaging.2017.03.007

Wang X, Huang Y, Li L, Wei Q (2012) TRAF3 negatively regulates calcineurin-NFAT pathway by targeting calcineurin B subunit for degradation. IUBMB Life 64(9):748–756. https://doi.org/10.1002/iub.1060

Wes PD, Easton A, Corradi J, Barten DM, Devidze N, DeCarr LB, Truong A, He A, Barrezueta NX, Polson C, Bourin C, Flynn ME, Keenan S, Lidge R, Meredith J, Natale J, Sankaranarayanan S, Cadelina GW, Albright CF, Cacace AM (2014) Tau overexpression impacts a neuroinflammation gene expression network perturbed in Alzheimer's disease. PLoS ONE 9(8):e106050. https://doi.org/10.1371/journal.pone.0106050

Wu C, MacLeod I, Su AI (2012) BioGPS and mygene.info: organizing online, gene-centric information. Nucleic Acids Res 41(D1). https://doi.org/10.1093/nar/gks1114

Xin J, Mark A, Afrasiabi C, Tsueng G, Juchler M, Gopal N, Stupp GS, Putman TE, Ainscough BJ, Griffith OL, Torkamani A, Whetzel PL, Mungall CJ, Mooney SD, Su AI, Wu C (2016) High-performance web services for querying gene and variant annotation. Genome Biol 17(1). https://doi.org/10.1186/s13059-016-0953-9

Zhou Z, Chan CH, Ma Q, Xu X, Xiao Z, Tan E-K (2011) The roles of amyloid precursor protein (APP) in Neurogenesis. Cell Adh Migr 5(4):280–292. https://doi.org/10.4161/cam.5.4.16986

Zuena AR, Casolini P, Lattanzi R, Maftei D (2019) Chemokines in alzheimer's disease: New insights into Prokineticins, chemokine-like proteins. Front Pharmacol 10. https://doi.org/10.3389/fphar.2019.00622